Analysis of $\Lambda_b^0 \to pK^-\mu^+\mu^-$ decays

The LHCb collaboration

E-mail: M.Kreps@warwick.ac.uk

ABSTRACT: The differential branching fraction and angular coefficients of $\Lambda_b^0 \to pK^-\mu^+\mu^-$ decays are measured in bins of the dimuon mass squared and dihadron mass. The analysis is performed using a data set corresponding to $9\,\text{fb}^{-1}$ of integrated luminosity collected with the LHCb detector between 2011 and 2018. The data are consistent with receiving contributions from a mixture of Λ resonances with different spin-parity quantum numbers. The angular coefficients show a pattern of vector-axial vector interference that is a characteristic of the type of flavour-changing neutral-current transition relevant for these decays.

Contents

1 Introduction

The decay of a Λ_b^0 baryon to a Λ resonance and a pair of oppositely charged muons is mediated by a b- to s-quark flavour-changing neutral-current (FCNC) transition. In the Standard Model (SM) of particle physics, such transitions are suppressed as they proceed via loop-order Feynman diagrams. In extensions of the SM, the decay rate and angular distribution can be significantly modified [1]. The rate and angular distribution of $\Lambda_b^0 \to \Lambda(1116)\mu^+\mu^-$ decays, where the $\Lambda(1116)$ baryon is the weakly decaying ground-state, have previously been studied by the LHCb and CDF collaborations [2–4].[1] While the properties of $\Lambda_b^0 \to \Lambda(1116)\mu^+\mu^-$ decays are consistent with SM expectations at the current level of experimental precision [5], tensions are seen in measurements of b- to s-quark FCNC transitions involving B^+, B^0 and B_s^0 mesons. The decay rates of these processes are found to be systematically below SM predictions [6–10]. Angular observables in $B^0 \to K^*(892)^0\mu^+\mu^-$ and $B^+ \to K^*(892)^+\mu^+\mu^-$ decays are also found to differ from expectations when the dimuon mass squared, q^2, is less than $8\,\mathrm{GeV}^2/c^4$ [11–18]. There is currently no conclusion on whether these discrepancies provide evidence for a genuine breakdown of the SM or are reflective of the challenges of calculating the rates of exclusive processes in a nonperturbative regime of QCD, see for

---

[1]The inclusion of charge-conjugate processes is implied throughout this paper unless explicitly stated.

example refs. [19–23]. It is therefore important to search for similar discrepancies in other hadronic systems, which require different theoretical treatments.

In this paper, $\Lambda_b^0 \to pK^-\mu^+\mu^-$ decays with intermediate Λ resonances decaying to pK^- are considered. Rare FCNC decays of a Λ_b^0 baryon to the $pK^-\mu^+\mu^-$ final state were first observed by the LHCb collaboration in ref. [24]. The differential branching fraction of the decay was measured in the range $0.1 < q^2 < 6.0\,\mathrm{GeV}^2/c^4$ in ref. [25]. Subsequently, the differential branching fraction to the narrowest strongly decaying state, the $\Lambda(1520)$ resonance, was measured in ref. [26] in bins of q^2. The full dihadron spectrum comprises a relatively large number of Λ states with different J^P quantum numbers. There are no accurate predictions of the differential decay rates of many of these states. Standard Model predictions, with reliable uncertainties, are only available for $\Lambda_b^0 \to \Lambda(1520)\mu^+\mu^-$ decays, based on Lattice QCD [27, 28] or dispersive bounds [29]. The hadronic form factors for transitions from Λ_b^0 baryons to other strongly decaying Λ resonances have only been estimated using a simplified quark model [30]. This paper presents a measurement of the branching fraction, and a first measurement of the angular distribution, of $\Lambda_b^0 \to pK^-\mu^+\mu^-$ decays. Coefficients of the angular distribution are determined using the formalism described in ref. [1].

The branching fraction and angular coefficients are measured in bins of q^2 and dihadron mass, m_{pK}. In q^2, the data are binned in the ranges 0.10–0.98, 1.1–2.0, 2.0–4.0, 4.0–6.0, 6.0–8.0, 11.0–12.5 and 15.0–17.5 GeV^2/c^4. In m_{pK}, the data are binned in the ranges 1.4359–1.5900, 1.59–1.75, 1.75–2.20 and 2.20–5.41 GeV/c^2. The first bin in m_{pK} isolates the narrow $\Lambda(1520)$ state, which is a prominent feature of the dihadron spectrum. The last bin in m_{pK} contains several broad Λ resonances whose properties are poorly known. At large q^2, the 1.4359–1.5900 and 1.59–1.75 GeV/c^2 bins are combined and the others are kinematically inaccessible. The q^2 regions between 0.98–1.10 and 12.5–15.0 GeV^2/c^4 are removed from the data sample as they contain contributions from ϕ and $\psi(2S)$ meson decays. Candidates with $8.0 < q^2 < 11.0\,\mathrm{GeV}^2/c^4$ are dominated by $\Lambda_b^0 \to J/\psi pK^-$ decays and are retained as a control sample.

At the LHC, Λ_b^0 baryons are observed to be produced with a net polarisation below 1% [31]. In this paper, they are treated as having zero polarisation in order to simplify the number of angular coefficients that need to be considered. In this case, the angular distribution of the decay can be described by three angles: θ_μ, the angle between the direction of the μ^+ (μ^-) in the $\mu^+\mu^-$ rest frame and the direction of the $\mu^+\mu^-$ pair in the Λ_b^0 ($\overline{\Lambda}_b^0$) rest frame; θ_p, the angle between the direction of the proton (antiproton) in the dihadron rest frame and the direction of the dihadron pair in the Λ_b^0 ($\overline{\Lambda}_b^0$) rest frame; ϕ, the angle between the $\mu^+\mu^-$ and dihadron decay planes in the Λ_b^0 rest frame. The resulting angular distribution is complex due to the contribution from a multitude of different Λ states, with different J^P quantum numbers, that decay to the same pK^- final state. For Λ states with $J \leq \frac{5}{2}$, the differential decay rate can be written in terms of a set of angular coefficients, $K_i(q^2, m_{pK}^2)$, as

$$\frac{\mathrm{d}^5\Gamma}{\mathrm{d}\boldsymbol{\Phi}} = \frac{3}{8\pi}\sum_{i=1}^{46} K_i(q^2, m_{pK}^2) f_i(\boldsymbol{\Omega})\,, \qquad (1.1)$$

where $\boldsymbol{\Phi} = (q^2, m_{pK}^2, \cos\theta_\mu, \cos\theta_p, \phi)$, $\boldsymbol{\Omega} = (\cos\theta_\mu, \cos\theta_p, \phi)$ and with the angular dependencies, $f_i(\boldsymbol{\Omega})$, given in table 1. The rate-averaged angular coefficients $\overline{K}_i$ in bins of q^2

and m_{pK}^2 are given by

$$\overline{K}_i = \int\limits_{\text{bin}} K_i(q^2, m_{pK}^2) \mathrm{d}q^2 \mathrm{d}m_{pK}^2 \bigg/ \int\limits_{\text{bin}} \frac{\mathrm{d}^2\Gamma}{\mathrm{d}q^2 \mathrm{d}m_{pK}^2} \mathrm{d}q^2 \mathrm{d}m_{pK}^2 \ . \tag{1.2}$$

Due to the large number of observables involved, the coefficients are determined using the method of moments (see e.g. ref. [32]) rather than by fitting the angular distribution of the data. Nonzero production polarisation of the Λ_b^0 baryons significantly increases the number of possible angular observables that can be measured but, due to the angular structure, does not affect the determination of the coefficients measured in this paper.

The data set used in this paper corresponds to $9\,\text{fb}^{-1}$ of integrated luminosity of pp collision data collected with the LHCb experiment between 2011 and 2018. This paper is organised as follows. Section 2 introduces the method used to determine the differential branching fraction and the $\overline{K}_i$ angular coefficients. Section 3 provides a description of the LHCb detector and its simulation. Section 4 describes the selection of candidates from the LHCb data set. Section 5 discusses the use of the $pK^-\mu^+\mu^-$ mass distribution, $m_{pK\mu\mu}$, to separate signal from background in the data set. Section 6 describes correcting weights that are needed to account for the nonuniform response of the detector in $\mathbf{\Phi}$. Sources of systematic uncertainty on the measurement of the branching fraction and angular coefficients are discussed in section 7. Results are presented in section 8 and summarised in section 9.

2 Methodology

The branching fraction of the $\Lambda_b^0 \to pK^-\mu^+\mu^-$ decay is measured relative to that of the $\Lambda_b^0 \to J/\psi pK^-$ decay, where the J/ψ meson subsequently decays to two oppositely charged muons. The differential branching fraction as a function of q^2 and m_{pK}^2 is

$$\frac{\mathrm{d}^2\mathcal{B}(\Lambda_b^0 \to pK^-\mu^+\mu^-)}{\mathrm{d}q^2\mathrm{d}m_{pK}^2} = \frac{N_{\Lambda_b^0 \to pK^-\mu^+\mu^-}}{N_{\Lambda_b^0 \to J/\psi pK^-}} \frac{\mathcal{B}(\Lambda_b^0 \to J/\psi pK^-)\mathcal{B}(J/\psi \to \mu^+\mu^-)}{\Delta(q^2, m_{pK}^2)} \ , \tag{2.1}$$

where N are the efficiency-corrected and background-subtracted yields of the decays in the relevant q^2 and m_{pK} ranges, and $\Delta(q^2, m_{pK}^2)$ is the area of the q^2 and m_{pK}^2 bin. For the $\Lambda_b^0 \to J/\psi pK^-$ decay, no restriction is made on the m_{pK} range. The branching fractions of the $\Lambda_b^0 \to J/\psi pK^-$ and $J/\psi \to \mu^+\mu^-$ decays are $(3.17\,^{+0.57}_{-0.45}) \times 10^{-2}$ [33] and $(5.961 \pm 0.033) \times 10^{-2}$ [34], respectively. Experimentally, the yields are calculated by summing over the candidates in the dataset with weight $w(\mathbf{\Phi})$,

$$N = \sum_{\text{event } n} w(\mathbf{\Phi}_n) \ . \tag{2.2}$$

The weights are given by the ratio $s_n/\varepsilon(\mathbf{\Phi}_n)$, where: $\varepsilon(\mathbf{\Phi}_n)$ is the candidate efficiency, which depends on the candidate's position in the five-dimensional phase space; while the s_n coefficients are calculated using the sPlot technique [35] from a fit to the four-body mass of the candidate, and are used to statistically subtract the background in the data set. For the $\Lambda_b^0 \to J/\psi pK^-$ decay, the sum runs over all candidates without restriction to a particular

i	$f_i(\boldsymbol{\Omega})$	i	$f_i(\boldsymbol{\Omega})$
1	$\frac{1}{\sqrt{3}}P_0^0(\cos\theta_p)P_0^0(\cos\theta_\mu)$	24	$\frac{1}{2}\sqrt{\frac{7}{3}}P_3^1(\cos\theta_p)P_1^1(\cos\theta_\mu)\cos\phi$
2	$P_0^0(\cos\theta_p)P_1^0(\cos\theta_\mu)$	25	$\frac{1}{2}P_4^1(\cos\theta_p)P_2^1(\cos\theta_\mu)\cos\phi$
3	$\sqrt{\frac{5}{3}}P_0^0(\cos\theta_p)P_2^0(\cos\theta_\mu)$	26	$\frac{3}{2\sqrt{5}}P_4^1(\cos\theta_p)P_1^1(\cos\theta_\mu)\cos\phi$
4	$P_1^0(\cos\theta_p)P_0^0(\cos\theta_\mu)$	27	$\frac{1}{3}\sqrt{\frac{11}{6}}P_5^1(\cos\theta_p)P_2^1(\cos\theta_\mu)\cos\phi$
5	$\sqrt{3}P_1^0(\cos\theta_p)P_1^0(\cos\theta_\mu)$	28	$\sqrt{\frac{11}{30}}P_5^1(\cos\theta_p)P_1^1(\cos\theta_\mu)\cos\phi$
6	$\sqrt{5}P_1^0(\cos\theta_p)P_2^0(\cos\theta_\mu)$	29	$\sqrt{\frac{5}{6}}P_1^1(\cos\theta_p)P_2^1(\cos\theta_\mu)\sin\phi$
7	$\sqrt{\frac{5}{3}}P_2^0(\cos\theta_p)P_0^0(\cos\theta_\mu)$	30	$\sqrt{\frac{3}{2}}P_1^1(\cos\theta_p)P_1^1(\cos\theta_\mu)\sin\phi$
8	$\sqrt{5}P_2^0(\cos\theta_p)P_1^0(\cos\theta_\mu)$	31	$\frac{5}{3\sqrt{6}}P_2^1(\cos\theta_p)P_2^1(\cos\theta_\mu)\sin\phi$
9	$\frac{5}{\sqrt{3}}P_2^0(\cos\theta_p)P_2^0(\cos\theta_\mu)$	32	$\sqrt{\frac{5}{6}}P_2^1(\cos\theta_p)P_1^1(\cos\theta_\mu)\sin\phi$
10	$\sqrt{\frac{7}{3}}P_3^0(\cos\theta_p)P_0^0(\cos\theta_\mu)$	33	$\frac{1}{6}\sqrt{\frac{35}{3}}P_3^1(\cos\theta_p)P_2^1(\cos\theta_\mu)\sin\phi$
11	$\sqrt{7}P_3^0(\cos\theta_p)P_1^0(\cos\theta_\mu)$	34	$\frac{1}{2}\sqrt{\frac{7}{3}}P_3^1(\cos\theta_p)P_1^1(\cos\theta_\mu)\sin\phi$
12	$\sqrt{\frac{35}{3}}P_3^0(\cos\theta_p)P_2^0(\cos\theta_\mu)$	35	$\frac{1}{2}P_4^1(\cos\theta_p)P_2^1(\cos\theta_\mu)\sin\phi$
13	$\sqrt{3}P_4^0(\cos\theta_p)P_0^0(\cos\theta_\mu)$	36	$\frac{3}{2\sqrt{5}}P_4^1(\cos\theta_p)P_1^1(\cos\theta_\mu)\sin\phi$
14	$3P_4^0(\cos\theta_p)P_1^0(\cos\theta_\mu)$	37	$\frac{1}{3}\sqrt{\frac{11}{6}}P_5^1(\cos\theta_p)P_2^1(\cos\theta_\mu)\sin\phi$
15	$\sqrt{15}P_4^0(\cos\theta_p)P_2^0(\cos\theta_\mu)$	38	$\sqrt{\frac{11}{30}}P_5^1(\cos\theta_p)P_1^1(\cos\theta_\mu)\sin\phi$
16	$\sqrt{\frac{11}{3}}P_5^0(\cos\theta_p)P_0^0(\cos\theta_\mu)$	39	$\frac{5}{12\sqrt{6}}P_2^2(\cos\theta_p)P_2^2(\cos\theta_\mu)\cos 2\phi$
17	$\sqrt{11}P_5^0(\cos\theta_p)P_1^0(\cos\theta_\mu)$	40	$\frac{1}{12}\sqrt{\frac{7}{6}}P_3^2(\cos\theta_p)P_2^2(\cos\theta_\mu)\cos 2\phi$
18	$\sqrt{\frac{55}{3}}P_5^0(\cos\theta_p)P_2^0(\cos\theta_\mu)$	41	$\frac{1}{12\sqrt{2}}P_4^2(\cos\theta_p)P_2^2(\cos\theta_\mu)\cos 2\phi$
19	$\sqrt{\frac{5}{6}}P_1^1(\cos\theta_p)P_2^1(\cos\theta_\mu)\cos\phi$	42	$\frac{1}{12}\sqrt{\frac{11}{42}}P_5^2(\cos\theta_p)P_2^2(\cos\theta_\mu)\cos 2\phi$
20	$\sqrt{\frac{3}{2}}P_1^1(\cos\theta_p)P_1^1(\cos\theta_\mu)\cos\phi$	43	$\frac{5}{12\sqrt{6}}P_2^2(\cos\theta_p)P_2^2(\cos\theta_\mu)\sin 2\phi$
21	$\frac{5}{3\sqrt{6}}P_2^1(\cos\theta_p)P_2^1(\cos\theta_\mu)\cos\phi$	44	$\frac{1}{12}\sqrt{\frac{7}{6}}P_3^2(\cos\theta_p)P_2^2(\cos\theta_\mu)\sin 2\phi$
22	$\sqrt{\frac{5}{6}}P_2^1(\cos\theta_p)P_1^1(\cos\theta_\mu)\cos\phi$	45	$\frac{1}{12\sqrt{2}}P_4^2(\cos\theta_p)P_2^2(\cos\theta_\mu)\sin 2\phi$
23	$\frac{1}{6}\sqrt{\frac{35}{3}}P_3^1(\cos\theta_p)P_2^1(\cos\theta_\mu)\cos\phi$	46	$\frac{1}{12}\sqrt{\frac{11}{42}}P_5^2(\cos\theta_p)P_2^2(\cos\theta_\mu)\sin 2\phi$

Table 1. Orthogonal basis functions for the angular terms $f_1(\boldsymbol{\Omega})$–$f_{46}(\boldsymbol{\Omega})$ that arise for unpolarised Λ_b^0 baryons decaying to Λ resonances with $J \le \frac{5}{2}$. Here, $P_l^m(\cos\theta)$ are associated Legendre polynomials. The basis follows ref. [1].

m_{pK} bin. The variance of N is given by

$$\text{Var}(N) = \sum_{\text{event } n} (w(\boldsymbol{\Phi}_n))^2 \,. \tag{2.3}$$

The angular observables can be determined by calculating the moments of the angular distribution. The rate-averaged angular coefficient across a bin is given by

$$\overline{K}_i = \frac{1}{N} \sum_{\text{event } n} w(\boldsymbol{\Phi}_n) f_i(\boldsymbol{\Omega}_n) \,, \tag{2.4}$$

as described in ref. [1]. These angular observables are extracted with respect to the angular basis given in table 1. Finally, the variance on the angular observables is given by

$$\text{Var}\left(\overline{K}_i\right) = \frac{1}{N^2} \sum_{\text{event } n} \left(w(\mathbf{\Phi}_n)\left(f_i(\mathbf{\Omega}_n) - \overline{K}_i\right)\right)^2 \ . \tag{2.5}$$

3   Detector and simulation

The LHCb detector [36, 37] is a single-arm forward spectrometer covering the pseudorapidity range $2 < \eta < 5$, designed for the study of b- or c-hadron decays. The detector includes a high-precision tracking system consisting of a silicon-strip vertex detector surrounding the pp interaction region, a large-area silicon-strip detector located upstream of a dipole magnet with a bending power of about $4\,\text{T}\,\text{m}$, and three stations of silicon-strip detectors and straw drift tubes placed downstream of the magnet. The tracking system provides a measurement of the momentum, p, of charged particles with a relative uncertainty better than 1% for $p < 200\,\text{GeV}/c$. Different types of charged hadrons are distinguished using information from two ring-imaging Cherenkov detectors. Muons are identified by a system comprising alternating layers of iron and multiwire proportional chambers. The online event selection is performed by a trigger, which comprises a hardware stage followed by two software stages.

Samples of simulated events are used to determine the efficiency, $\varepsilon(\mathbf{\Phi})$, and to study sources of specific backgrounds. In the simulation, pp collisions are generated using PYTHIA [38] with a specific LHCb configuration [39]. Decays of unstable particles are described by EVTGEN [40], with final-state radiation generated using PHOTOS [41]. The EVTGEN generator does not provide models for $\Lambda_b^0 \to pK^-\mu^+\mu^-$ and $\Lambda_b^0 \to J/\psi pK^-$ decays that are able to describe the full decay structure. Instead, the Λ_b^0 baryons are decayed according to phase-space availability. The $\Lambda_b^0 \to J/\psi pK^-$ decays are weighted to reproduce the amplitude structure determined in ref. [58]. The interaction of the generated particles with the detector, and its response, are implemented using the GEANT4 toolkit [42, 43] as described in ref. [44]. The simulated samples are corrected for known differences between data and simulation in the Λ_b^0 production kinematics. Percent-level corrections are also applied to the efficiency of the hardware trigger and to the tracking and muon identification efficiencies. These corrections are derived from control samples of $B^+ \to J/\psi K^+$ decays in the data [45]. The particle identification (PID) information for hadrons is corrected by replacing the simulated response with values from cleanly selected samples of protons and kaons with similar kinematic properties to the data of interest [46, 47].

4   Selection

The analysis uses data triggered in the hardware stage by either a single high transverse momentum muon or by a pair of muons with a large transverse momentum product. The first software stage requires an event to contain at least one good-quality track with significant displacement from every pp collision vertex (PV) and large transverse momentum. In the second stage, this track is combined with one or more other tracks and filtered according to topological criteria [48, 49]. Candidates are formed by combining two muons of opposite charge with a proton and a kaon. The muons and hadrons are required to have good-quality

tracks, have a significant impact parameter (IP) with respect to every PV and form a common vertex with a good vertex-fit quality. The Λ_b^0 candidate must have a significant transverse momentum and be significantly displaced from every PV. The candidate is assumed to originate from the PV with which it has the smallest IP. The candidates are required to have an IP consistent with zero and a momentum vector aligned with the direction between the origin and decay vertices.

A lower threshold on the angle between the directions of any pair of charged particles is applied to remove cases where a single charged particle results in multiple reconstructed tracks. Additional requirements are applied to remove specific sources of background. The most dangerous sources of background arise from decays with similar topologies, where one or more particles are incorrectly identified. For example, $B_s^0 \to K^+K^-\mu^+\mu^-$ decays, where the K^+ is mistakenly identified as a proton. Such decays are suppressed by requiring additional particle identification criteria if the dihadron and four-body mass combination are consistent with originating from a different decay with a similar topology. The kaon to proton misidentification probability after particle identification requirements is typically at the percent level. Such requirements also remove background contributions from $\Lambda_b^0 \to pK^-\mu^+\mu^-$ decays where the proton is mistakenly identified as a kaon and vice versa. Four-body hadronic b-hadron decays form a negligible source of background.

There is also a potentially large background source from semileptonic $\Lambda_b^0 \to \Lambda_c^+\mu^-\bar{\nu}_\mu$ decays, where the Λ_c^+ baryon decays to $pK^-\pi^+$ and the π^+ is mistakenly identified as a muon. Such decays are suppressed by vetoing candidates where the $pK^-\pi^+$ mass is consistent with the Λ_c^+ baryon mass, after assigning the π^+ mass hypothesis to the μ^+ candidate. Processes involving two semileptonic decays, such as $\Lambda_b^0 \to \Lambda_c^+\mu^-\bar{\nu}_\mu$ with $\Lambda_c^+ \to pK^-\mu^+\nu_\mu$, populate the low $pK^-\mu^+\mu^-$ mass region and can be safely ignored in the analysis. Semileptonic decays of B_s^0 mesons, such as $B_s^0 \to D_s^-\mu^+\nu_\mu$ with $D_s^- \to K^+K^-\mu^-\bar{\nu}_\mu$, are suppressed by requiring that the candidate $K^+K^-\mu^+\mu^-$ mass, formed by assigning the kaon mass hypothesis to the proton candidate, is larger than $5\,\mathrm{GeV}/c^2$.

After suppressing the major sources of specific backgrounds, the remaining background contribution is dominated by random combinations of protons, kaons, and two oppositely charged muons. A significant fraction of the background is found to have a dihadron system consistent with coming from $\phi \to K^+K^-$ decays, where a kaon is mistakenly identified as a proton. Additional particle identification criteria are applied to suppress this background. The remaining background is further suppressed using a multivariate classifier, a boosted decision tree [50], trained to separate simulated signal decays from candidates selected from an upper mass sideband of the data. The classifier uses features of the data with low correlations to the phase-space variables and the $pK^-\mu^+\mu^-$ mass: the fit quality of the Λ_b^0 decay vertex, the angle between the Λ_b^0 momentum and its reconstructed flight direction, the p_{T} of the Λ_b^0 candidate, and the consistency of the candidate with originating from a PV. The response of the classifier is validated on the $\Lambda_b^0 \to J/\psi pK^-$ data and simulation samples. The classifier working point is chosen to maximise the expected signal significance in the data. The chosen working point removes 98% of the combinatorial background in the upper mass sideband and retains 74% of simulated signal decays.

5 Mass distribution

The sPlot procedure [35] is used to statistically disentangle the signal and remaining background. An unbinned maximum-likelihood fit is performed to the $m_{pK\mu\mu}$ distribution in the different bins using the ZFIT software package [51]. The signal component is described by a Gaussian distribution with power law tails on both sides of the peak [52], and the combinatorial background is modelled by an exponential distribution. The tail parameters of the signal shape are determined using the simulated samples. The peak position and width parameters of the signal are also obtained from simulation and corrected based on fits to the $\Lambda_b^0 \to J/\psi p K^-$ control sample. All bins share the peak position in simulation, as well as the correction factors for the peak position and width in data. For the $\Lambda_b^0 \to J/\psi p K^-$ sample, the other signal parameters are independent between the different m_{pK} bins. For the other q^2 bins, the other signal parameters are shared between bins with the same q^2 but different m_{pK} values. Due to the larger size of the $\Lambda_b^0 \to J/\psi p K^-$ sample, the models are modified to better describe the shapes seen in the data: the signal shape is modified to include sigmoid activation functions on the left- and right-hand side of the distribution to account for the effect of the finite dimuon mass window on $m_{pK\mu\mu}$; and the background shape is modified by multiplying it by

$$\Theta(m_{pK\mu\mu} - m_{\mathrm{thr}})(m_{pK\mu\mu} - m_{\mathrm{thr}})^\delta \,, \tag{5.1}$$

where Θ is the Heaviside step function, m_{thr} is the smallest allowed $pK^-\mu^+\mu^-$ mass and is given by the sum of the known J/ψ mass [34] and m_{pK}, and δ is a parameter that controls the turn-on of the shape from the threshold.

Figures 1 and 2 show the $m_{pK\mu\mu}$ distribution of the candidates in the different q^2 and m_{pK} bins. The distributions are overlaid with the result of the fit. In the $6 < q^2 < 8\,\mathrm{GeV}^2/c^4$ bin, the range of the $m_{pK\mu\mu}$ distribution is reduced to remove background from poorly reconstructed $\Lambda_b^0 \to J/\psi p K^-$ decays that would otherwise pollute the low mass region. Table 4 in the appendix contains the yields of signal and background obtained from the fits. The angular observables are determined for every bin of q^2 and m_{pK} that has a significant signal contribution. For $2.20 < m_{pK} < 5.41\,\mathrm{GeV}/c^2$, and the bin with $1.1 < q^2 < 2.0\,\mathrm{GeV}^2/c^4$ and $1.4359 < m_{pK} < 1.5900\,\mathrm{GeV}/c^2$, the signal yields are so small that the angular observables cannot be reliably determined.

6 Efficiency model

The efficiency in $\boldsymbol{\Phi}$ is parameterised by

$$\varepsilon(\boldsymbol{\Phi}) = \sum_{hijkl} e_{hijkl} P_h(m'_{pK}) P_i(m'_{\mu\mu}) P_j(\cos\theta_p) P_k(\cos\theta_\mu) \cos(l\phi) \,, \tag{6.1}$$

where $P_n(x)$ are Legendre polynomials of order n, the e_{hijkl} are a set of coefficients, and m'_{pK} and $m'_{\mu\mu}$ are a mapping of the dihadron and dimuon masses to a square with range $[-1, +1]$. This model makes no assumptions about the factorisation of the different observables. Legendre polynomials and $\cos(l\phi)$ dependencies are used since these form an orthogonal basis. As a result, the coefficients of the efficiency model are determined using the method
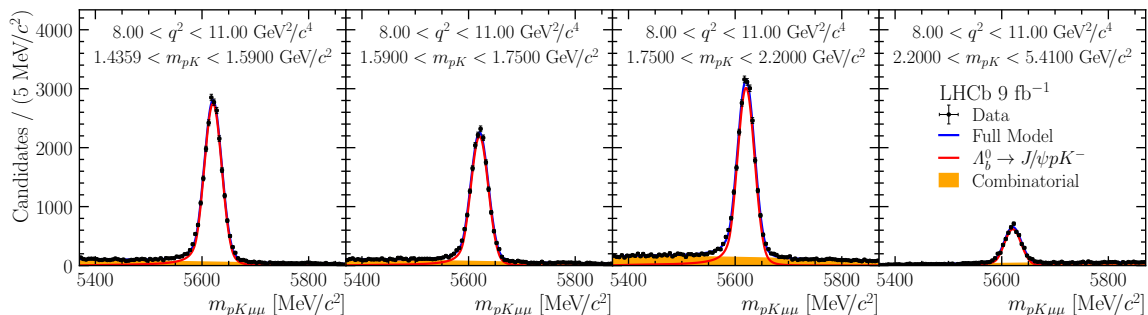
Figure 1. Mass distribution of selected $\Lambda_b^0 \to J/\psi pK^-$ candidates in bins of m_{pK}. The data are overlaid with the result of the fit described in the text.

of moments applied to the phase-space simulation samples. The efficiency is parameterised using polynomials of up-to and including: order five for the transformed masses, $m'_{\mu\mu}$ and m'_{pK}; order four for $\cos\theta_p$; and order four for $\cos\theta_\mu$. The angle ϕ is described by functions up-to $\cos(3\phi)$. The normalisation of the efficiency is arbitrary, and on average candidates are assigned values of 1.0. If $\varepsilon(\mathbf{\Phi}) < 0.15$, candidates are assigned an efficiency of 0.15 to avoid introducing large weights when determining the observables. This only affects a small number of candidates that all sit in the sidebands of the data. The impact of the minimum efficiency requirement is considered as a source of systematic uncertainty.

The shape of $\varepsilon(\mathbf{\Phi})$ arises from kinematic and geometrical requirements in the selection and reconstruction of the proton, kaon and muons. The shape in $\cos\theta_\mu$ is symmetric as the detection asymmetry between positively and negatively charged muons is negligible [53], therefore odd order contributions are not considered in the model. Conversely, the shape in $\cos\theta_p$ is asymmetric due to the difference between the proton and kaon mass, leading to a momentum imbalance between the particles in the detector, and due to different momentum-dependent efficiencies of the PID requirements. For $\cos\theta_p$, both odd and even order contributions are used. The efficiency tends to be largest at intermediate q^2 and lower at the q^2 extremes. At small q^2, the muons typically have smaller momentum and p_{T}, and are either not reconstructed, or do not meet the requirements of the hardware stage of the trigger. At large q^2, the hadrons are almost at rest in the Λ_b^0 rest frame and have small IP, and do not meet the requirements of the software trigger or offline selection.

The efficiency model is validated by inspecting the agreement between one-dimensional projections of the model and the simulation samples. The agreement in the five-dimensional space is also checked using a multivariate classifier trained to separate the simulation sample and pseudoexperiments generated from the efficiency model. Several different combinations of polynomial orders are found to give a similar description of the simulated sample. This set of models is used to assign a systematic uncertainty on $\varepsilon(\mathbf{\Phi})$.

7 Statistical and systematic uncertainties

The statistical uncertainty on the branching fraction measurements and the angular observables are determined using the variances defined in section 2. The appropriateness of the variance, as a measure of the uncertainty, is verified with pseudoexperiments. An alternative
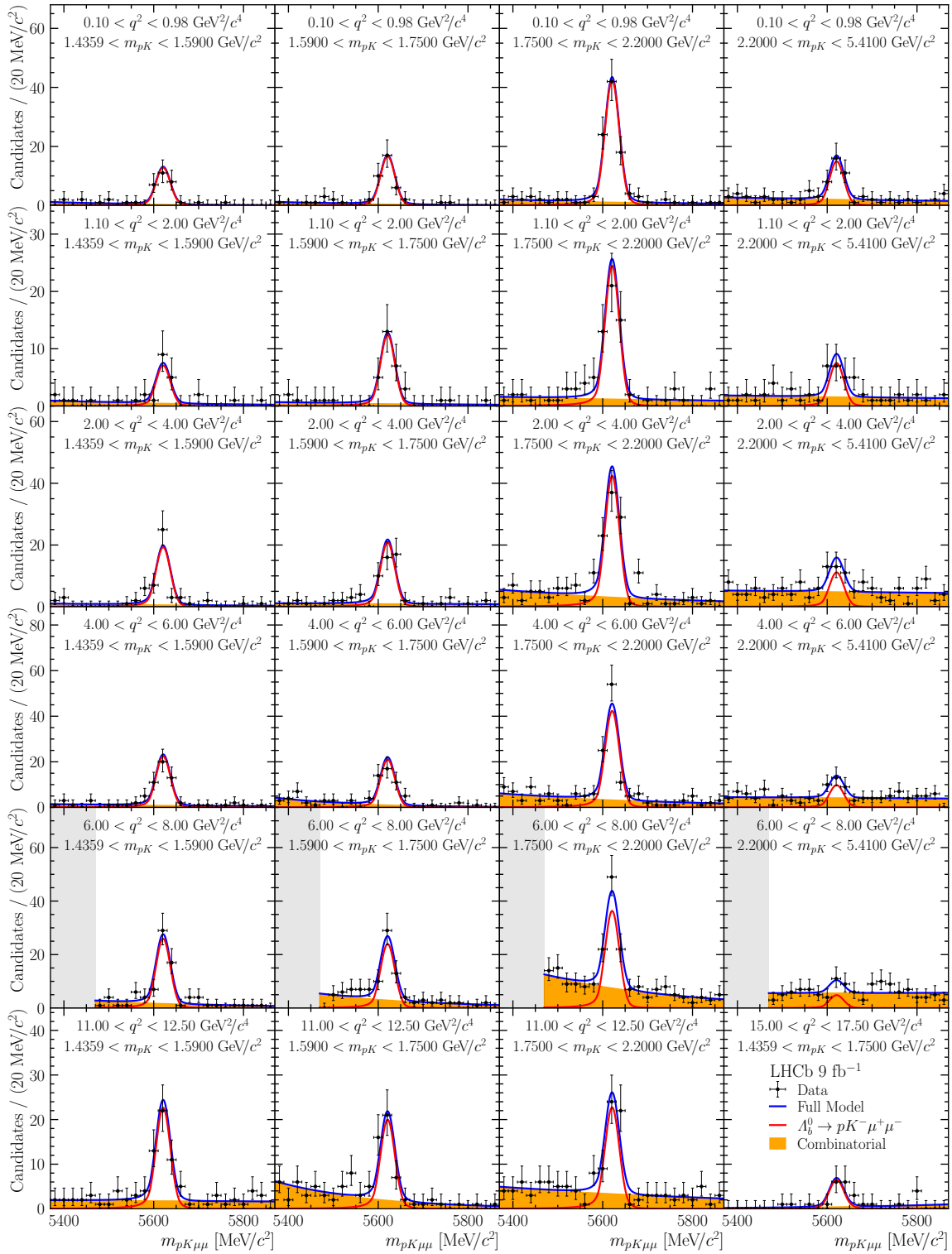
Figure 2. Mass distributions of selected $\Lambda_b^0 \to pK^-\mu^+\mu^-$ decay candidates in bins of m_{pK} and q^2. The data are overlaid with the result of the fit described in the text. The shaded regions are populated by poorly reconstructed $\Lambda_b^0 \to J/\psi pK^-$ decays and are excluded from the analysis.

Source of systematic uncertainty	$\mathrm{d}^2\mathcal{B}/\mathrm{d}q^2\mathrm{d}m_{pK}^2$	$\overline{K}_i$
$\mathcal{B}(\Lambda_b^0 \to J/\psi pK^-)$	1.03 (0.35–1.58)	—
Efficiency model (sample size)	0.09 (0.03–0.25)	0.07 (0.01–0.40)
Efficiency model (polynomial order)	0.10 (0.03–0.47)	0.08 (0.01–1.15)
Efficiency model (minimum value)	0.01 (0.00–0.22)	0.00 (0.00–0.99)
Efficiency model (Λ_c^+ veto)	0.01 (0.00–0.16)	0.00 (0.00–0.27)
Mass model (signal)	0.02 (0.00–0.18)	0.01 (0.00–0.17)
Mass model (background)	0.05 (0.00–0.95)	0.01 (0.00–0.20)
Mass model (sample size)	0.01 (0.00–0.09)	0.00 (0.00–0.05)
Peaking backgrounds	0.02 (0.00–0.09)	0.01 (0.00–0.16)
Resolution	0.00 (0.00–0.02)	0.00 (0.00–0.18)
Simulation corrections (PID)	0.02 (0.00–0.08)	0.01 (0.00–0.36)
Simulation corrections (hadronisation)	0.00 (0.00–0.02)	0.00 (0.00–0.01)
Simulation corrections (kinematic)	0.02 (0.00–0.06)	0.01 (0.00–0.08)

Table 2. Summary of different sources of systematic uncertainty on the differential branching fraction and angular coefficients, relative to the statistical uncertainty on the measurements. The values correspond to the median over all of the measured observables and bins. The absolute range is given in parentheses.

estimate, obtained by bootstrapping the data set [54] and repeating the determination of the different observables, is also considered. The two determinations give comparable results for bins that are well populated, but the variance is found to have better coverage in poorly populated bins and to cover correctly for the observables presented in this paper.

Several sources of systematic uncertainties are considered. For the differential branching fraction, the dominant contribution arises from the knowledge of the branching fraction of the $\Lambda_b^0 \to J/\psi pK^-$ decay. The largest systematic uncertainty on the angular coefficients stems from the knowledge of the efficiency model. Table 2 provides a summary of the different sources of systematic uncertainty. The total systematic uncertainty on the observables is determined by summing the individual sources in quadrature.

Four sources of systematic uncertainty are evaluated for the efficiency model. The first source is due to the limited size of the simulation sample. To assess the systematic impact of this limitation, the simulated sample is bootstrapped 100 times and the determination of the efficiency model is repeated. The observables are recalculated for each alternative efficiency model and the widths of the resulting distributions of the observables are taken as systematic uncertainties. The second source is due to the choice of the truncation order of the polynomials used in the efficiency model. The size of this effect is quantified by determining different efficiency models by either increasing or decreasing the polynomial order of the different dimensions by one, considering only the models that provide a similarly good description of the data to the baseline model. The observables are then determined using these alternative efficiency models. The largest deviation from the default value among

the models is assigned as the systematic uncertainty on each observable. Only an increase and decrease of one is considered because very high orders of the polynomial can lead to local regions with small or negative efficiencies in $\varepsilon(\boldsymbol{\Phi})$. The third source is due to the choice of the minimum efficiency. The impact of this choice is estimated by repeating the analysis on a single pseudoexperiment with a large sample size with the minimum efficiency set to 0.01. The difference in the value of observables obtained using the default minimum and the new minimum efficiency is taken as systematic uncertainty. The Λ_c^+ veto removes a very narrow region of phase space, which is difficult to model with polynomial functions. Because the efficiency of the Λ_c^+ veto is 99.8% on signal simulation samples, and no candidates fall in this region in data, this veto is not applied when determining the efficiency shape. The fourth source of uncertainty accounts for this choice and is also determined using a single large pseudoexperiment. The difference in absolute value between the observables calculated from the sample when neglecting or including the Λ_c^+ veto is taken as systematic uncertainty.

Three sources of systematic uncertainty are evaluated for the mass models. The first source is due to the statistical uncertainty on the signal line shape. This uncertainty is assessed by varying the line shape parameters within their uncertainties, repeating the fits to the data and determining new values for the observables. The width of the resulting distributions of the observables are taken as systematic uncertainties. The second and third sources are due to the choice of signal and background model. The systematic effect of the model choice is estimated using pseudoexperiments generated according to an alternative signal or background model. The observables are then determined using the baseline signal and background models and the resulting bias is assigned as a source of systematic uncertainty. For the signal, an alternative shape based on a modified asymmetric Apollonios function is used [55]. For the background, a polynomial dependence is used with parameters determined from a sample selected with a looser multivariate classifier requirement. The uncertainty due to different signal and background line shapes is largest for $1.75 < m_{pK} < 2.20\,\mathrm{GeV}/c^2$.

Contributions from misidentified backgrounds with the same topology as the signal are small and neglected in the analysis. To estimate a systematic uncertainty due to omitting these backgrounds, a pseudoexperiment is generated with a large sample size according to the baseline signal and background models. Additional background contributions from misidentified particles are introduced at the expected level. The observables are then determined using the baseline signal and background models and the resulting bias is assigned as a systematic uncertainty. As little is known of the structure of the $B_s^0 \to K^- K^+ \mu^+ \mu^-$ and $B^0 \to K^+ \pi^- \mu^+ \mu^-$ decays, aside from in the region around the ϕ and $K^*(892)^0$ resonances, the additional candidates are selected from the data after applying alternative particle identification requirements.

The resolution of the measured particle momentum has little impact on the measured angular observables and is neglected in the analysis. To assess the impact of this choice, a pseudoexperiment with a large sample size is generated in which θ_μ, θ_p and ϕ are smeared according to the resolutions on the angles determined from simulation. The observables are then determined using the baseline model and the bias on the observables is assigned as a systematic uncertainty.

The determination of the efficiency is based on simulation samples that are calibrated to better describe the data. The overall value of the calibrating weight is dominated by the correction of the Λ_b^0 production kinematics. The kinematic correction is designed to correctly reproduce the p_{T} dependence of the Λ_b^0 production fraction relative to B^0 and B^+ mesons measured in refs. [56] and [57], as well as the kinematic distributions of B^0 and B^+ mesons in the data. A systematic uncertainty on the correction to the Λ_b^0 kinematics is assessed in two ways. First, the measurements in refs. [56] and [57] are varied within their uncertainties and new efficiency models are determined for each variation. The observables are determined in data using the resulting alternate efficiency models. The width of the resulting distributions of values of the different observables is assigned as a systematic uncertainty. Second, the correction weights are also extended to include the detector occupancy. The analysis is then repeated and the change in the values of the observables is assigned as a systematic uncertainty. A systematic uncertainty on the hadron identification is also estimated by evaluating the efficiency model using information sampled from an alternative set of calibration samples. Overall, the systematic uncertainties related to the calibration are small.

8 Results and discussion

Table 3 gives the differential branching fraction for every bin. The precision in most bins is limited by the knowledge of the $\Lambda_b^0 \to J/\psi pK^-$ branching fraction. Figure 3 shows the results in bins of q^2 and m_{pK}. The branching fraction as a function of q^2 in the first m_{pK} bin is compatible with the results presented in ref. [26]. The branching fraction obtained by summing the contributions from different q^2 and m_{pK} bins over the ranges $0.1 < q^2 < 6.0\,\mathrm{GeV}^2/c^4$ and $m_{pK} < 2.6\,\mathrm{GeV}/c^2$ is also compatible with the measurement presented in ref. [25]. The variation of the differential branching fraction with q^2 obtained in this paper does not agree with predictions based on a quark model [30] in any of the m_{pK} bins. The quark model predictions typically yield much smaller branching fractions at low-q^2 than seen in the data. A direct interpretation of the differences between the differential branching fraction in bins of m_{pK} and the resonance spectra in $\Lambda_b^0 \to J/\psi pK^-$ [58] and $\Lambda_b^0 \to pK^-\gamma$ [59] decays is difficult, due to the unknown interference pattern between the states in this analysis. The results are, however, qualitatively similar, with a variety of different resonances contributing to the total rate. The pattern is also consistent with the available phase space in the different decays.

Figures 5–10 in the appendix show the values of the complete set of angular observables. Tabulated values of all of the observables are available as attached supplementary material. Figure 4 shows the forward-backward asymmetries of the lepton and hadron systems computed from the observables. The lepton- and hadron-side forward-backward asymmetries correspond to

$$A_{\mathrm{FB}}^{\mu} = \frac{3}{2}\overline{K}_2 \quad \text{and} \quad A_{\mathrm{FB}}^{p} = \frac{3}{2}\overline{K}_4 - \frac{\sqrt{21}}{8}\overline{K}_{10} + \frac{\sqrt{33}}{16}\overline{K}_{16}\,, \tag{8.1}$$

respectively [1]. The lepton-side asymmetry is sensitive to interference between vector and axial-vector contributions to the decay. This asymmetry shows the same pattern observed in $B^0 \to K^{*0}\mu^+\mu^-$ decays with a characteristic sign-change between low and high q^2 [12]. Note that the sign of the lepton-side asymmetry in this paper differs due to the angular basis

m_{pK} / q^2	[1.4359, 1.5900]	[1.59, 1.75]	[1.75, 2.20]	[2.20, 5.41]
[0.10, 0.98]	$5.22 \pm 1.21 \pm 0.43 \pm 0.98$	$8.22 \pm 1.69 \pm 0.38 \pm 1.54$	$7.24 \pm 0.92 \pm 0.52 \pm 1.36$	$0.46 \pm 0.13 \pm 0.14 \pm 0.09$
[1.1, 2.0]	$3.05 \pm 1.45 \pm 0.51 \pm 0.57$	$6.27 \pm 1.71 \pm 0.40 \pm 1.18$	$4.24 \pm 0.78 \pm 0.16 \pm 0.80$	$0.16 \pm 0.09 \pm 0.02 \pm 0.03$
[2.0, 4.0]	$4.56 \pm 0.90 \pm 0.26 \pm 0.86$	$4.50 \pm 0.86 \pm 0.21 \pm 0.84$	$3.44 \pm 0.47 \pm 0.08 \pm 0.64$	$0.12 \pm 0.05 \pm 0.02 \pm 0.02$
[4.0, 6.0]	$4.72 \pm 0.76 \pm 0.15 \pm 0.89$	$4.29 \pm 0.73 \pm 0.20 \pm 0.81$	$3.36 \pm 0.41 \pm 0.07 \pm 0.63$	$0.11 \pm 0.03 \pm 0.02 \pm 0.02$
[6.0, 8.0]	$5.08 \pm 0.76 \pm 0.12 \pm 0.95$	$4.65 \pm 0.79 \pm 0.34 \pm 0.87$	$2.56 \pm 0.36 \pm 0.05 \pm 0.48$	$0.04 \pm 0.02 \pm 0.01 \pm 0.01$
[11, 12.5]	$5.32 \pm 0.86 \pm 0.20 \pm 1.00$	$4.53 \pm 0.80 \pm 0.16 \pm 0.85$	$1.67 \pm 0.28 \pm 0.03 \pm 0.31$	—
[15.0, 17.5]	$0.59 \pm 0.19 \pm 0.07 \pm 0.11$		—	—

Table 3. Differential branching fraction, $\mathrm{d}^2\mathcal{B}/\mathrm{d}q^2\mathrm{d}m_{pK}^2$, in units of $10^{-8}\,\mathrm{GeV}^{-4}c^8$ in bins of q^2 and m_{pK}. The first uncertainty is statistical, the second systematic, and the third due to the uncertainty on the $\Lambda_b^0 \to J/\psi pK^-$ branching fraction. The bin ranges are given in GeV/c^2 for m_{pK} and in GeV^2/c^4 for q^2.
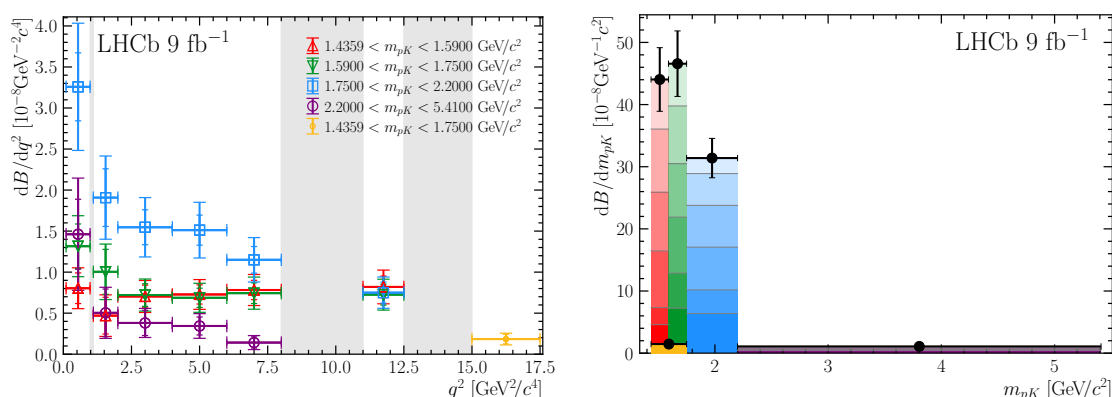
Figure 3. Differential branching fraction as a function of (left) q^2 and (right) m_{pK}. The stacked contributions with different shading in the right figure indicate the contributions from the different q^2 bins. The darker hue corresponds to smaller values of q^2.

used. A large hadron-side asymmetry is seen in many of the q^2 and m_{pK} bins, especially for $1.75 < m_{pK} < 2.20\,\mathrm{GeV}/c^2$. The hadron-side asymmetry is sensitive to the interference between states with different quantum numbers.

9 Summary

An analysis of the rate and angular distribution of $\Lambda_b^0 \to pK^-\mu^+\mu^-$ decays, using data collected with LHCb detector between 2011–2018, has been presented. The analysis results in a first measurement of the differential branching fraction of the $\Lambda_b^0 \to pK^-\mu^+\mu^-$ decay across its entire phase space, in bins of the dihadron mass and q^2. The decay rate is dominated by contributions from resonances at low dihadron masses. This paper also provides a first measurement of a complete set of angular observables in $\Lambda_b^0 \to pK^-\mu^+\mu^-$ decays for Λ states with spin less than $\frac{5}{2}$. These measurements are only provided in bins with sufficient signal yield. The angular coefficients indicate the presence of interference between states with different quantum numbers. They also show the pattern of interference between vector and axial-vector contributions that is characteristic of this type of rare FCNC decay. The
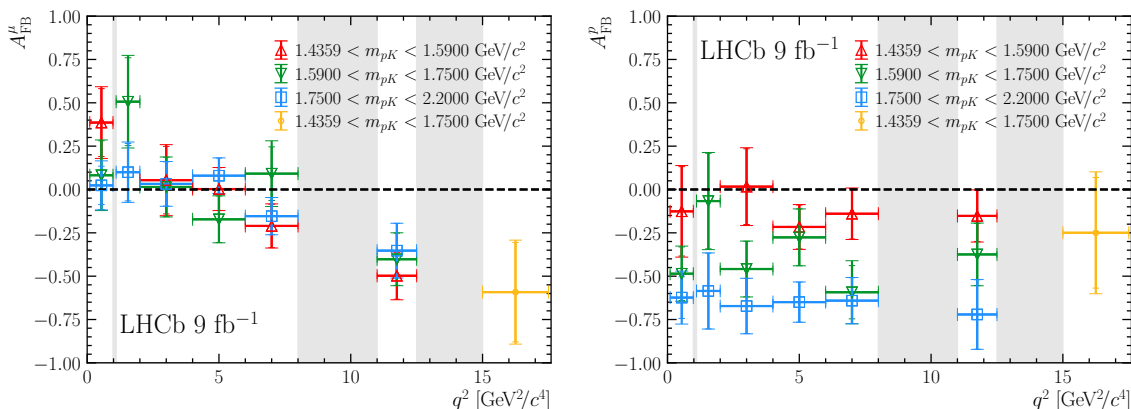
Figure 4. Values of the (left) dimuon forward-backward asymmetry and (right) dihadron forward-backward asymmetry in bins of q^2 and m_{pK}.

pattern of measurements appears consistent with SM expectations. However, a detailed interpretation of the results requires a more complete understanding of the hadronic system and the different contributing states.

Acknowledgments

q^2 [GeV^2/c^4]	m_{pK} [GeV/c^2]	Signal	Background
0.10–0.98	1.4359–1.5900	27^{+6}_{-5}	11^{+4}_{-3}
	1.59–1.75	35^{+7}_{-6}	13^{+5}_{-4}
	1.75–2.20	90^{+10}_{-10}	29^{+7}_{-6}
	2.20–5.41	32^{+7}_{-6}	51^{+8}_{-8}
1.1–2.0	1.4359–1.5900	15^{+5}_{-4}	13^{+4}_{-4}
	1.59–1.75	27^{+6}_{-5}	10^{+4}_{-3}
	1.75–2.20	52^{+8}_{-8}	31^{+7}_{-6}
	2.20–5.41	16^{+6}_{-5}	40^{+8}_{-7}
2.0–4.0	1.4359–1.5900	42^{+7}_{-7}	15^{+5}_{-4}
	1.59–1.75	45^{+8}_{-7}	24^{+6}_{-5}
	1.75–2.20	92^{+11}_{-11}	81^{+11}_{-10}
	2.20–5.41	24^{+7}_{-7}	121^{+12}_{-12}
4.0–6.0	1.4359–1.5900	48^{+8}_{-7}	23^{+6}_{-5}
	1.59–1.75	45^{+8}_{-7}	36^{+7}_{-6}
	1.75–2.20	91^{+11}_{-10}	87^{+11}_{-10}
	2.20–5.41	21^{+7}_{-6}	105^{+12}_{-11}
6.0–8.0	1.4359–1.5900	55^{+9}_{-8}	31^{+7}_{-6}
	1.59–1.75	51^{+9}_{-8}	54^{+9}_{-8}
	1.75–2.20	77^{+11}_{-10}	137^{+14}_{-13}
	2.20–5.41	10^{+6}_{-5}	113^{+12}_{-11}
11.0–12.5	1.4359–1.5900	49^{+8}_{-8}	44^{+8}_{-7}
	1.59–1.75	43^{+8}_{-7}	59^{+9}_{-8}
	1.75–2.20	49^{+9}_{-8}	86^{+11}_{-10}
15.0–17.0	1.4359–1.5900	14^{+5}_{-4}	12^{+4}_{-4}

Table 4. Signal and background yields obtained from fitting $pK^-\mu^+\mu^-$ mass distributions in the data in the different bins of q^2 and m_{pK}.

A   Signal and background yields

Table 4 provides the observed signal and background yield in each of the q^2 and m_{pK} bins from the unbinned extended maximum-likelihood fit to $pK^-\mu^+\mu^-$ distributions. The uncertainties on the yields are calculated from the profile likelihood [60].

B   Angular observables

The values of the $\overline{K}_2$–$\overline{K}_{46}$ angular observables in the different q^2 and m_{pK} bins are provided in figures 5–10.
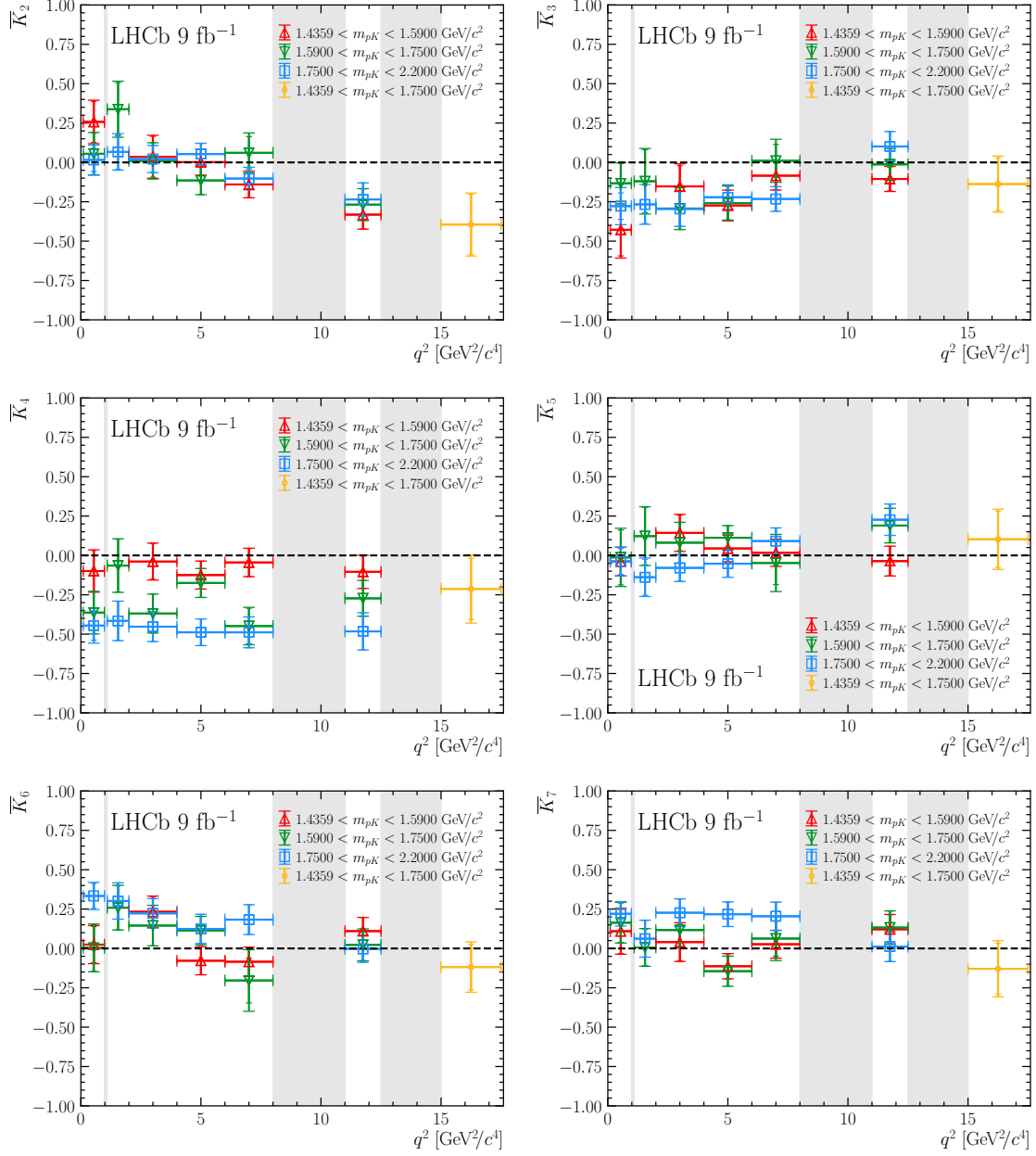
Figure 5. Values of $\overline{K}_2$–$\overline{K}_7$ in bins of q^2 and m_{pK}.
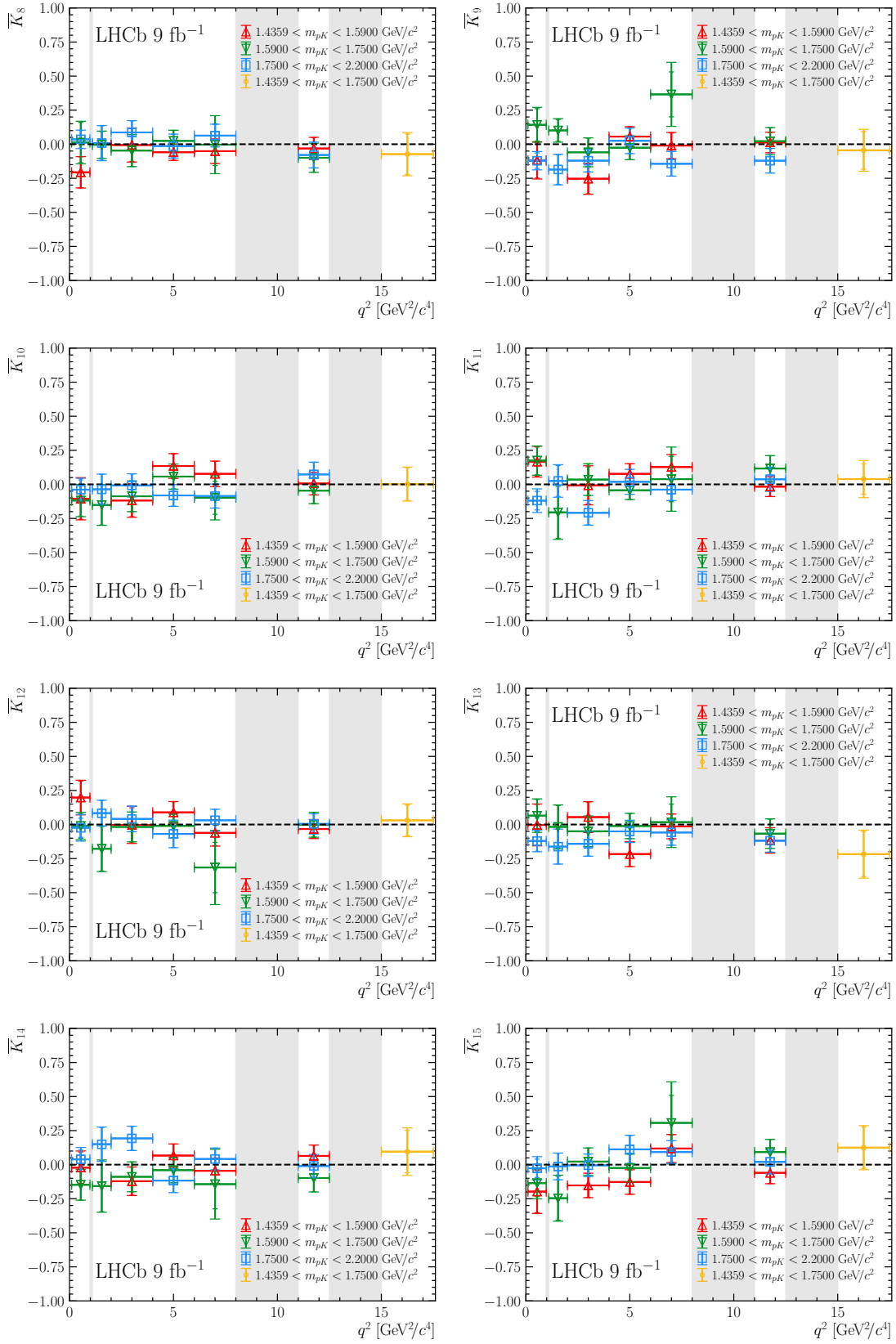
Figure 6. Values of $\overline{K}_8$–$\overline{K}_{15}$ in bins of q^2 and m_{pK}.
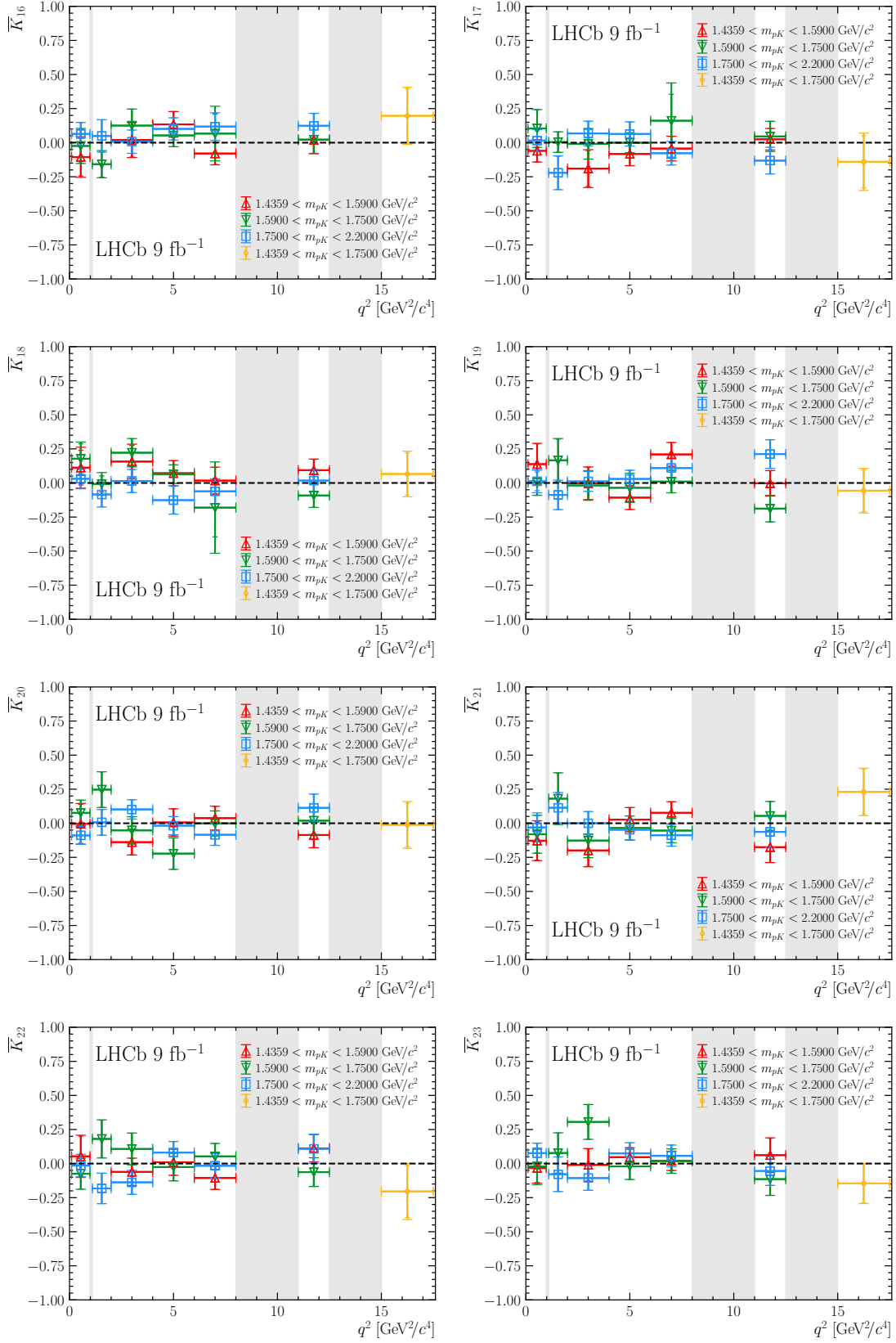
Figure 7. Values of $\overline{K}_{16}$–$\overline{K}_{23}$ in bins of q^2 and m_{pK}.
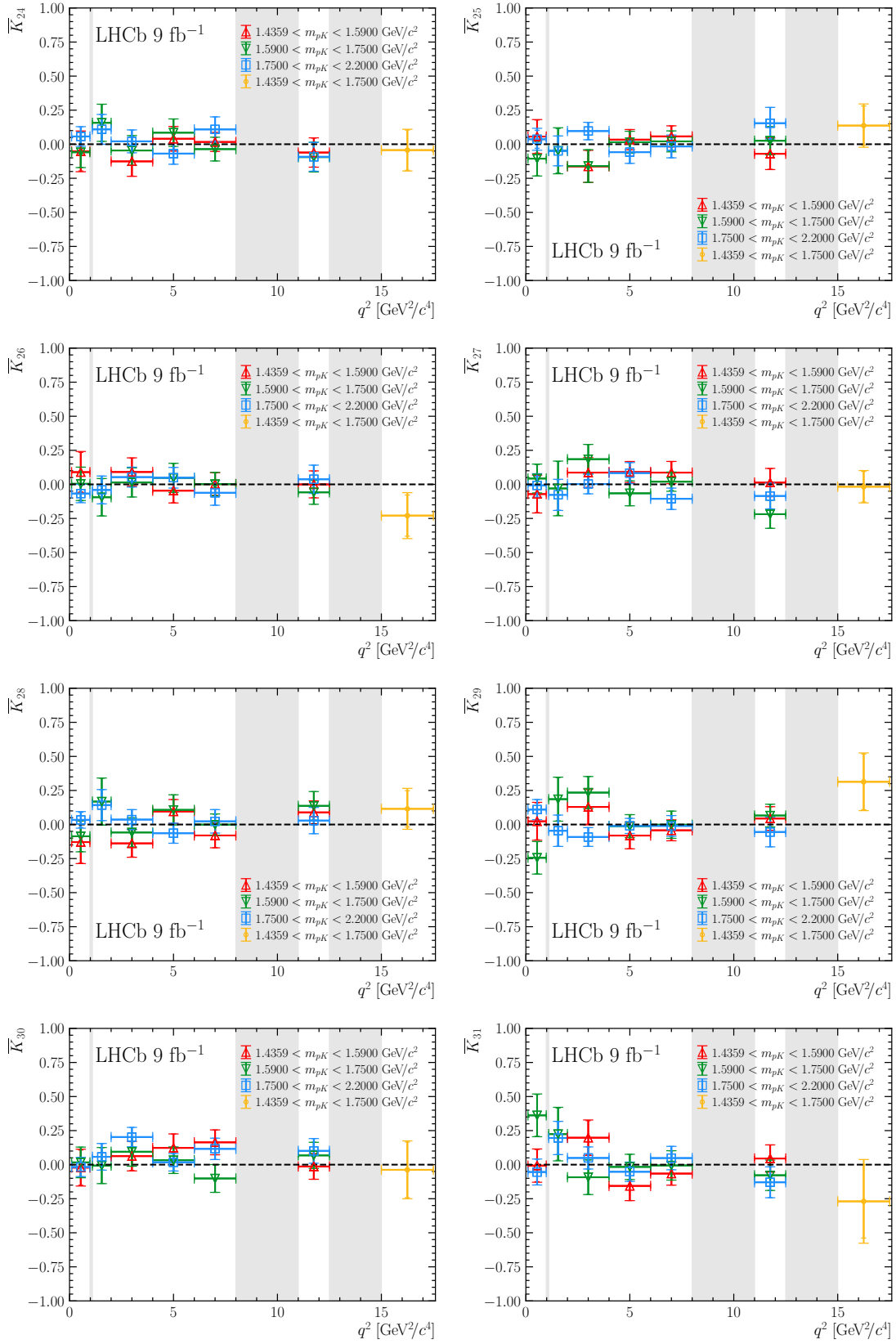
Figure 8. Values of $\overline{K}_{24}$–$\overline{K}_{31}$ in bins of q^2 and m_{pK}.
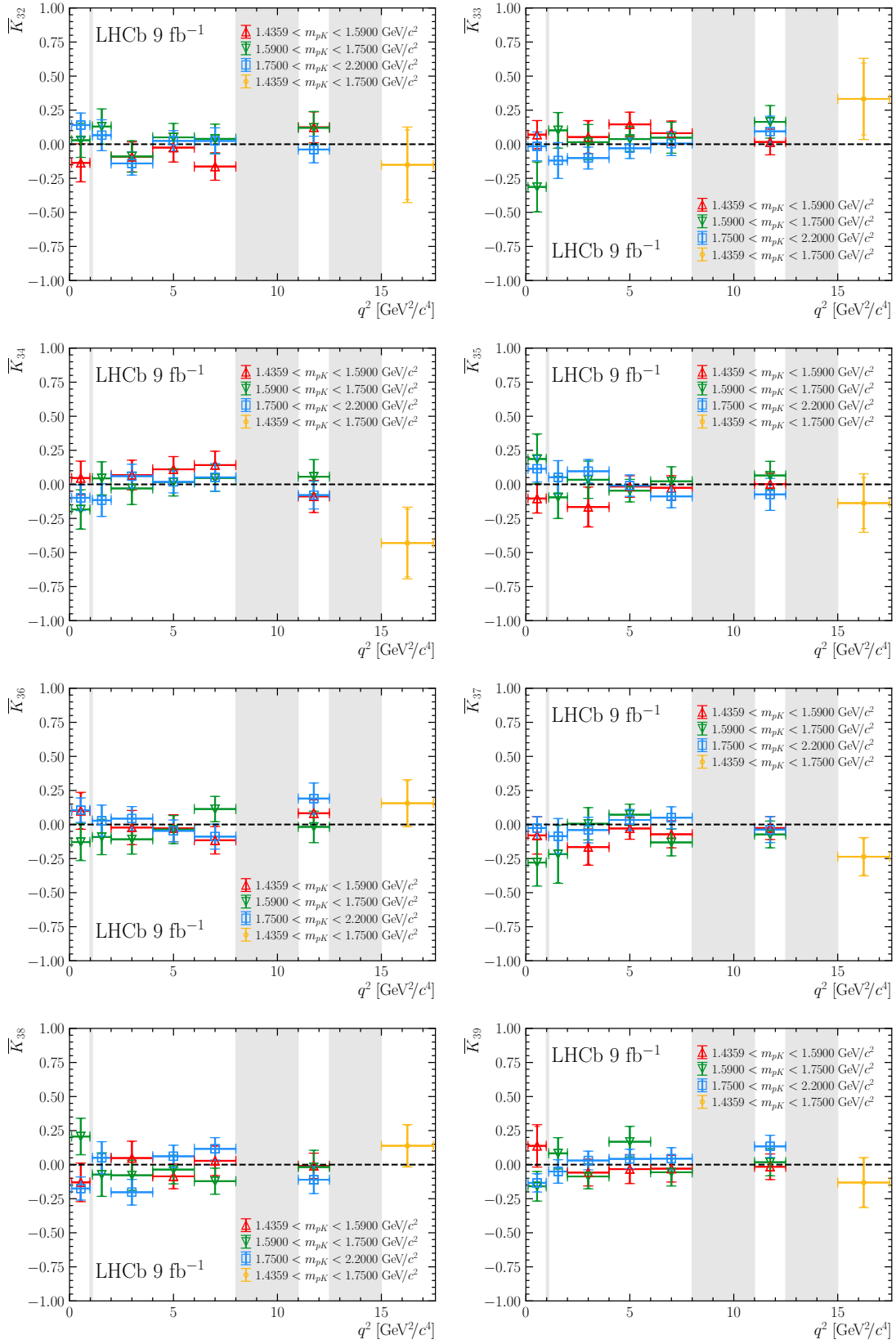
Figure 9. Values of $\overline{K}_{32}$–$\overline{K}_{39}$ in bins of q^2 and m_{pK}.
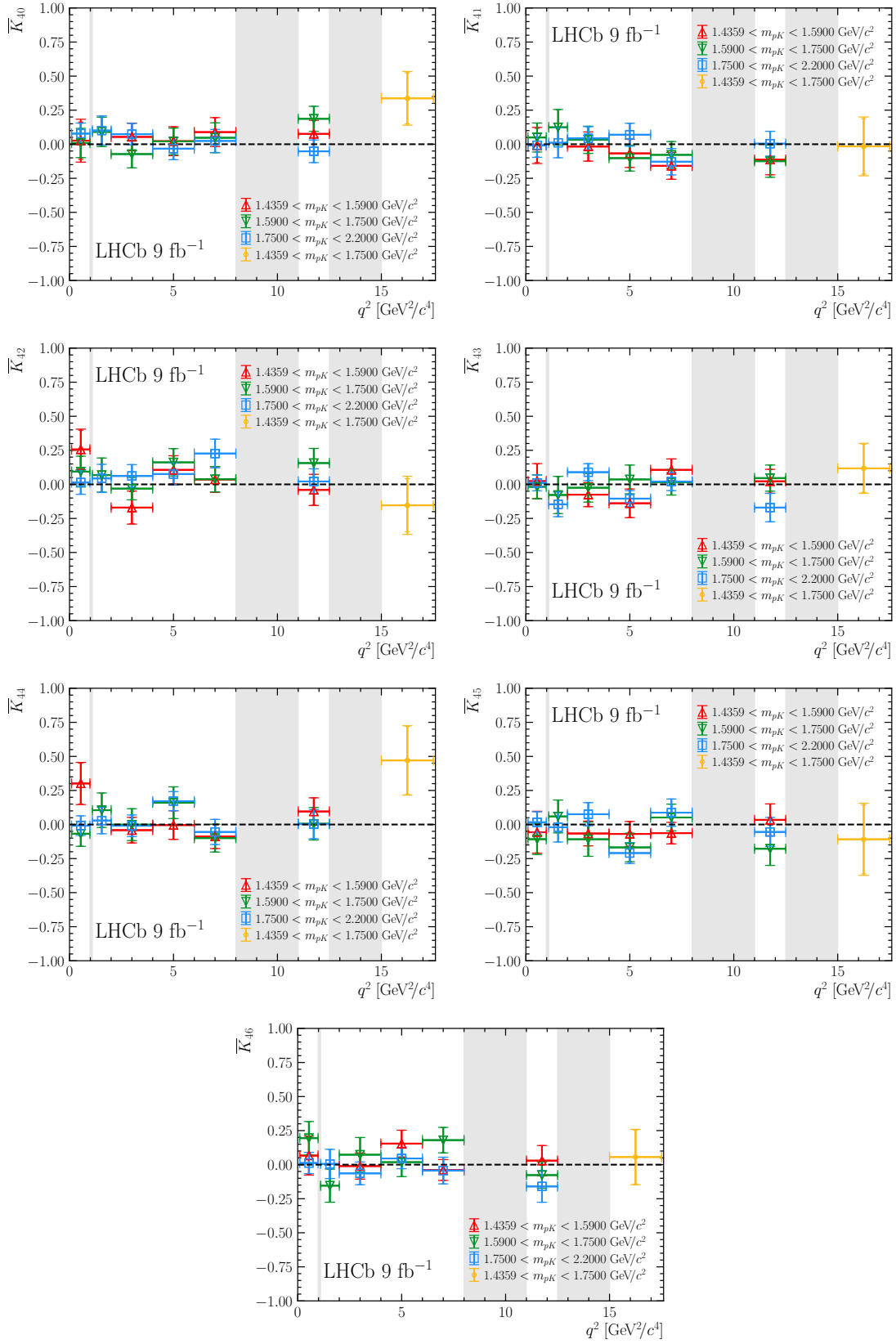
Figure 10. Values of $\overline{K}_{40}$–$\overline{K}_{46}$ in bins of q^2 and m_{pK}.

Data Availability Statement. This article has data included as electronic supplementary material.

Code Availability Statement. This article has no associated code or the code will not be deposited.

Open Access. This article is distributed under the terms of the Creative Commons Attribution License ([CC-BY4.0](#)), which permits any use, distribution and reproduction in any medium, provided the original author(s) and source are credited.

References

[1] A. Beck, T. Blake and M. Kreps, *Angular distribution of $\Lambda_b^0 \to pK^-\ell^+\ell^-$ decays comprising Λ resonances with spin $\leq 5/2$*, *JHEP* **02** (2023) 189 [arXiv:2210.09988] [InSPIRE].

[2] LHCb collaboration, *Differential branching fraction and angular analysis of $\Lambda_b^0 \to \Lambda\mu^+\mu^-$ decays*, *JHEP* **06** (2015) 115 [*Erratum ibid.* **09** (2018) 145] [arXiv:1503.07138] [InSPIRE].

[3] LHCb collaboration, *Angular moments of the decay $\Lambda_b^0 \to \Lambda\mu^+\mu^-$ at low hadronic recoil*, *JHEP* **09** (2018) 146 [arXiv:1808.00264] [InSPIRE].

[4] CDF collaboration, *Observation of the baryonic flavor-changing neutral current decay $\Lambda_b \to \Lambda\mu^+\mu^-$*, *Phys. Rev. Lett.* **107** (2011) 201802 [arXiv:1107.3753] [InSPIRE].

[5] T. Blake, S. Meinel and D. van Dyk, *Bayesian analysis of $b \to s\mu^+\mu^-$ Wilson coefficients using the full angular distribution of $\Lambda_b \to \Lambda(\to p\,\pi^-)\mu^+\mu^-$ decays*, *Phys. Rev. D* **101** (2020) 035023 [arXiv:1912.05811] [InSPIRE].

[6] LHCb collaboration, *Measurements of the S-wave fraction in $B^0 \to K^+\pi^-\mu^+\mu^-$ decays and the $B^0 \to K^*(892)^0\mu^+\mu^-$ differential branching fraction*, *JHEP* **11** (2016) 047 [*Erratum ibid.* **04** (2017) 142] [arXiv:1606.04731] [InSPIRE].

[7] LHCb collaboration, *Branching fraction measurements of the rare $B_s^0 \to \phi\mu^+\mu^-$ and $B_s^0 \to f_2'(1525)\mu^+\mu^-$ decays*, *Phys. Rev. Lett.* **127** (2021) 151801 [arXiv:2105.14007] [InSPIRE].

[8] CMS collaboration, *Angular analysis of the decay $B^+ \to K^+\mu^+\mu^-$ in proton-proton collisions at $\sqrt{s} = 8$ TeV*, *Phys. Rev. D* **98** (2018) 112011 [arXiv:1806.00636] [InSPIRE].

[9] BELLE collaboration, *Test of lepton flavor universality and search for lepton flavor violation in $B \to K\ell\ell$ decays*, *JHEP* **03** (2021) 105 [arXiv:1908.01848] [InSPIRE].

[10] BaBar collaboration, *Measurement of branching fractions and rate asymmetries in the rare decays $B \to K^{(*)}l^+l^-$*, *Phys. Rev. D* **86** (2012) 032012 [arXiv:1204.3933] [InSPIRE].

[11] LHCb collaboration, *Differential branching fractions and isospin asymmetries of $B \to K^{(*)}\mu^+\mu^-$ decays*, *JHEP* **06** (2014) 133 [arXiv:1403.8044] [InSPIRE].

[12] LHCb collaboration, *Measurement of CP-averaged observables in the $B^0 \to K^{*0}\mu^+\mu^-$ decay*, *Phys. Rev. Lett.* **125** (2020) 011802 [arXiv:2003.04831] [InSPIRE].

[13] LHCb collaboration, *Angular analysis of the $B^+ \to K^{*+}\mu^+\mu^-$ decay*, *Phys. Rev. Lett.* **126** (2021) 161802 [arXiv:2012.13241] [InSPIRE].

[14] LHCb collaboration, *Angular analysis of the rare decay $B_s^0 \to \phi\mu^+\mu^-$*, *JHEP* **11** (2021) 043 [arXiv:2107.13428] [InSPIRE].

[15] LHCb collaboration, *Comprehensive analysis of local and nonlocal amplitudes in the $B^0 \to K^{*0}\mu^+\mu^-$ decay*, *JHEP* **09** (2024) 026 [arXiv:2405.17347] [InSPIRE].

[16] CMS collaboration, *Angular analysis of the decay $B^+ \to K^*(892)^+\mu^+\mu^-$ in proton-proton collisions at $\sqrt{s} = 8$ TeV*, *JHEP* **04** (2021) 124 [arXiv:2010.13968] [INSPIRE].

[17] CMS collaboration, *Measurement of angular parameters from the decay $B^0 \to K^{*0}\mu^+\mu^-$ in proton-proton collisions at $\sqrt{s} = 8$ TeV*, *Phys. Lett. B* **781** (2018) 517 [arXiv:1710.02846] [INSPIRE].

[18] ATLAS collaboration, *Angular analysis of $B_d^0 \to K^*\mu^+\mu^-$ decays in pp collisions at $\sqrt{s} = 8$ TeV with the ATLAS detector*, *JHEP* **10** (2018) 047 [arXiv:1805.04000] [INSPIRE].

[19] M. Ciuchini et al., *On flavourful Easter eggs for new physics hunger and lepton flavour universality violation*, *Eur. Phys. J. C* **77** (2017) 688 [arXiv:1704.05447] [INSPIRE].

[20] B. Capdevila et al., *Patterns of new physics in $b \to s\ell^+\ell^-$ transitions in the light of recent data*, *JHEP* **01** (2018) 093 [arXiv:1704.05340] [INSPIRE].

[21] N. Gubernari, M. Reboud, D. van Dyk and J. Virto, *Improved theory predictions and global analysis of exclusive $b \to s\mu^+\mu^-$ processes*, *JHEP* **09** (2022) 133 [arXiv:2206.03797] [INSPIRE].

[22] T. Hurth, F. Mahmoudi and S. Neshatpour, *B anomalies in the post $R_{K^{(*)}}$ era*, *Phys. Rev. D* **108** (2023) 115037 [arXiv:2310.05585] [INSPIRE].

[23] M. Bordone, G. isidori, S. Mächler and A. Tinari, *Short- vs. long-distance physics in $B \to K^{(*)}\ell^+\ell^-$: a data-driven analysis*, *Eur. Phys. J. C* **84** (2024) 547 [arXiv:2401.18007] [INSPIRE].

[24] LHCb collaboration, *Observation of the decay $\Lambda_b^0 \to pK^-\mu^+\mu^-$ and a search for CP violation*, *JHEP* **06** (2017) 108 [arXiv:1703.00256] [INSPIRE].

[25] LHCb collaboration, *Test of lepton universality with $\Lambda_b^0 \to pK^-\ell^+\ell^-$ decays*, *JHEP* **05** (2020) 040 [arXiv:1912.08139] [INSPIRE].

[26] LHCb collaboration, *Measurement of the $\Lambda_b^0 \to \Lambda(1520)\mu^+\mu^-$ differential branching fraction*, *Phys. Rev. Lett.* **131** (2023) 151801 [arXiv:2302.08262] [INSPIRE].

[27] S. Meinel and G. Rendon, *$\Lambda_b \to \Lambda^*(1520)\ell^+\ell^-$ form factors from lattice QCD*, *Phys. Rev. D* **103** (2021) 074505 [arXiv:2009.09313] [INSPIRE].

[28] S. Meinel and G. Rendon, *$\Lambda_c \to \Lambda^*(1520)$ form factors from lattice QCD and improved analysis of the $\Lambda_b \to \Lambda^*(1520)$ and $\Lambda_b \to \Lambda_c^*(2595, 2625)$ form factors*, *Phys. Rev. D* **105** (2022) 054511 [arXiv:2107.13140] [INSPIRE].

[29] Y. Amhis, M. Bordone and M. Reboud, *Dispersive analysis of $\Lambda_b \to \Lambda(1520)$ local form factors*, *JHEP* **02** (2023) 010 [arXiv:2208.08937] [INSPIRE].

[30] L. Mott and W. Roberts, *Rare dileptonic decays of Λ_b in a quark model*, *Int. J. Mod. Phys. A* **27** (2012) 1250016 [arXiv:1108.6129] [INSPIRE].

[31] LHCb collaboration, *Measurement of the $\Lambda_b^0 \to J/\psi\Lambda$ angular distribution and the Λ_b^0 polarisation in pp collisions*, *JHEP* **06** (2020) 110 [arXiv:2004.10563] [INSPIRE].

[32] F. Beaujean, M. Chrząszcz, N. Serra and D. van Dyk, *Extracting angular observables without a likelihood and applications to rare decays*, *Phys. Rev. D* **91** (2015) 114012 [arXiv:1503.04100] [INSPIRE].

[33] LHCb collaboration, *Study of the production of Λ_b^0 and $\overline{B}^0$ hadrons in pp collisions and first measurement of the $\Lambda_b^0 \to J/\psi pK^-$ branching fraction*, *Chin. Phys. C* **40** (2016) 011001 [arXiv:1509.00292] [INSPIRE].

[34] PARTICLE DATA GROUP collaboration, *Review of particle physics*, *Phys. Rev. D* **110** (2024) 030001 [INSPIRE].

[35] M. Pivk and F.R. Le Diberder, *SPlot: a statistical tool to unfold data distributions*, *Nucl. Instrum. Meth. A* **555** (2005) 356 [physics/0402083] [INSPIRE].

[36] LHCb collaboration, *The LHCb detector at the LHC*, 2008 *JINST* **3** S08005 [INSPIRE].

[37] LHCb collaboration, *LHCb detector performance*, *Int. J. Mod. Phys. A* **30** (2015) 1530022 [arXiv:1412.6352] [INSPIRE].

[38] T. Sjöstrand, S. Mrenna and P.Z. Skands, *A brief introduction to PYTHIA 8.1*, *Comput. Phys. Commun.* **178** (2008) 852 [arXiv:0710.3820] [INSPIRE].

[39] LHCb collaboration, *Handling of the generation of primary events in Gauss, the LHCb simulation framework*, *J. Phys. Conf. Ser.* **331** (2011) 032047 [INSPIRE].

[40] D.J. Lange, *The EvtGen particle decay simulation package*, *Nucl. Instrum. Meth. A* **462** (2001) 152 [INSPIRE].

[41] N. Davidson, T. Przedzinski and Z. Was, *PHOTOS interface in C++: technical and physics documentation*, *Comput. Phys. Commun.* **199** (2016) 86 [arXiv:1011.0937] [INSPIRE].

[42] J. Allison et al., *GEANT4 developments and applications*, *IEEE Trans. Nucl. Sci.* **53** (2006) 270 [INSPIRE].

[43] GEANT4 collaboration, *GEANT4 — a simulation toolkit*, *Nucl. Instrum. Meth. A* **506** (2003) 250 [INSPIRE].

[44] LHCb collaboration, *The LHCb simulation application, Gauss: design, evolution and experience*, *J. Phys. Conf. Ser.* **331** (2011) 032023 [INSPIRE].

[45] LHCb collaboration, *Measurement of the track reconstruction efficiency at LHCb*, 2015 *JINST* **10** P02007 [arXiv:1408.1251] [INSPIRE].

[46] A. Poluektov, *Kernel density estimation of a multidimensional efficiency profile*, 2015 *JINST* **10** P02011 [arXiv:1411.5528] [INSPIRE].

[47] R. Aaij et al., *Selection and processing of calibration samples to measure the particle identification performance of the LHCb experiment in run 2*, *EPJ Tech. Instrum.* **6** (2019) 1 [arXiv:1803.00824] [INSPIRE].

[48] V.V. Gligorov and M. Williams, *Efficient, reliable and fast high-level triggering using a bonsai boosted decision tree*, 2013 *JINST* **8** P02013 [arXiv:1210.6861] [INSPIRE].

[49] T. Likhomanenko et al., *LHCb topological trigger reoptimization*, *J. Phys. Conf. Ser.* **664** (2015) 082025 [arXiv:1510.00572] [INSPIRE].

[50] T. Chen and C. Guestrin, *XGBoost: a scalable tree boosting system*, arXiv:1603.02754 [DOI:10.1145/2939672.2939785] [INSPIRE].

[51] J. Eschle, A. Puig Navarro, R. Silva Coutinho and N. Serra, *zfit: scalable pythonic fitting*, *SoftwareX* **11** (2020) 100508 [arXiv:1910.13429] [INSPIRE].

[52] T. Skwarnicki, *A study of the radiative CASCADE transitions between the Upsilon-Prime and Upsilon resonances*, Ph.D. thesis, INP, Cracow, Poland (1986) [INSPIRE].

[53] LHCb collaboration, *Measurement of the flavour-specific CP-violating asymmetry a_{sl}^s in B_s^0 decays*, *Phys. Lett. B* **728** (2014) 607 [arXiv:1308.1048] [INSPIRE].

[54] B. Efron, *Bootstrap methods: another look at the Jackknife*, *Annals Statist.* **7** (1979) 1 [INSPIRE].

[55] D. Martínez Santos and F. Dupertuis, *Mass distributions marginalized over per-event errors*, *Nucl. Instrum. Meth. A* **764** (2014) 150 [`arXiv:1312.5000`] [INSPIRE].

[56] LHCb collaboration, *Measurement of b-hadron production fractions in 7 TeV pp collisions*, *Phys. Rev. D* **85** (2012) 032008 [`arXiv:1111.2357`] [INSPIRE].

[57] LHCb collaboration, *Measurement of b hadron fractions in 13 TeV pp collisions*, *Phys. Rev. D* **100** (2019) 031102 [`arXiv:1902.06794`] [INSPIRE].

[58] LHCb collaboration, *Observation of $J/\psi p$ resonances consistent with pentaquark states in $\Lambda_b^0 \to J/\psi K^- p$ decays*, *Phys. Rev. Lett.* **115** (2015) 072001 [`arXiv:1507.03414`] [INSPIRE].

[59] LHCb collaboration, *Amplitude analysis of the $\Lambda_b^0 \to pK^-\gamma$ decay*, *JHEP* **06** (2024) 098 [`arXiv:2403.03710`] [INSPIRE].

[60] F. James and M. Roos, *Minuit: a system for function minimization and analysis of the parameter errors and correlations*, *Comput. Phys. Commun.* **10** (1975) 343 [INSPIRE].

The LHCb collaboration

R. Aaij [37], A.S.W. Abdelmotteleb [56], C. Abellan Beteta[50], F. Abudinén [56], T. Ackernley [60], A. A. Adefisoye [68], B. Adeva [46], M. Adinolfi [54], P. Adlarson [81], C. Agapopoulou [14], C.A. Aidala [82], Z. Ajaltouni[11], S. Akar [65], K. Akiba [37], P. Albicocco [27], J. Albrecht [19,g], F. Alessio [48], M. Alexander [59], Z. Aliouche [62], P. Alvarez Cartelle [55], R. Amalric [16], S. Amato [3], J.L. Amey [54], Y. Amhis [14,48], L. An [6], L. Anderlini [26], M. Andersson [50], A. Andreianov [43], P. Andreola [50], M. Andreotti [25], D. Andreou [68], A. Anelli [30,p], D. Ao [7], F. Archilli [36,v], M. Argenton [25], S. Arguedas Cuendis [9,48], A. Artamonov [43], M. Artuso [68], E. Aslanides [13], R. Ataíde Da Silva [49], M. Atzeni [64], B. Audurier [15], D. Bacher [63], I. Bachiller Perea [10], S. Bachmann [21], M. Bachmayer [49], J.J. Back [56], P. Baladron Rodriguez [46], V. Balagura [15], W. Baldini [25], L. Balzani [19], H. Bao [7], J. Baptista de Souza Leite [60], C. Barbero Pretel [46,12], M. Barbetti [26], I. R. Barbosa [69], R.J. Barlow [62], M. Barnyakov [24], S. Barsuk [14], W. Barter [58], M. Bartolini [55], J. Bartz [68], J.M. Basels [17], S. Bashir [39], G. Bassi [34,s], B. Batsukh [5], P. B. Battista[14], A. Bay [49], A. Beck [56], M. Becker [19], F. Bedeschi [34], I.B. Bediaga [2], N. A. Behling [19], S. Belin [46], V. Bellee [50], K. Belous [43], I. Belov [28], I. Belyaev [35], G. Benane [13], G. Bencivenni [27], E. Ben-Haim [16], A. Berezhnoy [43], R. Bernet [50], S. Bernet Andres [44], A. Bertolin [32], C. Betancourt [50], F. Betti [58], J. Bex [55], Ia. Bezshyiko [50], J. Bhom [40], M.S. Bieker [19], N.V. Biesuz [25], P. Billoir [16], A. Biolchini [37], M. Birch [61], F.C.R. Bishop [10], A. Bitadze [62], A. Bizzeti [], T. Blake [56], F. Blanc [49], J.E. Blank [19], S. Blusk [68], V. Bocharnikov [43], J.A. Boelhauve [19], O. Boente Garcia [15], T. Boettcher [65], A. Bohare [58], A. Boldyrev [43], C.S. Bolognani [78], R. Bolzonella [25,m], N. Bondar [43], A. Bordelius [48], F. Borgato [32,q], S. Borghi [62], M. Borsato [30,p], J.T. Borsuk [40], S.A. Bouchiba [49], M. Bovill [63], T.J.V. Bowcock [60], A. Boyer [48], C. Bozzi [25], A. Brea Rodriguez [49], N. Breer [19], J. Brodzicka [40], A. Brossa Gonzalo [46,56,45,†], J. Brown [60], D. Brundu [31], E. Buchanan[58], A. Buonaura [50], L. Buonincontri [32,q], A.T. Burke [62], C. Burr [48], J.S. Butter [55], J. Buytaert [48], W. Byczynski [48], S. Cadeddu [31], H. Cai[73], A. C. Caillet[16], R. Calabrese [25,m], S. Calderon Ramirez [9], L. Calefice [45], S. Cali [27], M. Calvi [30,p], M. Calvo Gomez [44], P. Camargo Magalhaes [2,z], J. I. Cambon Bouzas [46], P. Campana [27], D.H. Campora Perez [78], A.F. Campoverde Quezada [7], S. Capelli [30], L. Capriotti [25], R. Caravaca-Mora [9], A. Carbone [24,k], L. Carcedo Salgado [46], R. Cardinale [28,n], A. Cardini [31], P. Carniti [30,p], L. Carus[21], A. Casais Vidal [64], R. Caspary [21], G. Casse [60], J. Castro Godinez [9], M. Cattaneo [48], G. Cavallero [25,48], V. Cavallini [25,m], S. Celani [21], D. Cervenkov [63], S. Cesare [29,o], A.J. Chadwick [60], I. Chahrour [82], M. Charles [16], Ph. Charpentier [48], E. Chatzianagnostou [37], M. Chefdeville [10], C. Chen [13], S. Chen [5], Z. Chen [7], A. Chernov [40], S. Chernyshenko [52], X. Chiotopoulos [78], V. Chobanova [80], S. Cholak [49], M. Chrzaszcz [40], A. Chubykin [43], V. Chulikov [43], P. Ciambrone [27], X. Cid Vidal [46], G. Ciezarek [48], P. Cifra [48], P.E.L. Clarke [58], M. Clemencic [48], H.V. Cliff [55], J. Closier [48], C. Cocha Toapaxi [21], V. Coco [48], J. Cogan [13], E. Cogneras [11], L. Cojocariu [42], P. Collins [48], T. Colombo [48], M. C. Colonna [19], A. Comerma-Montells [45], L. Congedo [23], A. Contu [31], N. Cooke [59], I. Corredoira [46], A. Correia [16], G. Corti [48], J.J. Cottee Meldrum[54], B. Couturier [48], D.C. Craik [50], M. Cruz Torres [2,h], E. Curras Rivera [49], R. Currie [58], C.L. Da Silva [67], S. Dadabaev [43], L. Dai [70], X. Dai [6], E. Dall'Occo [19], J. Dalseno [46],

C. D'Ambrosio [48], J. Daniel [11], A. Danilina [43], P. d'Argent [23], A. Davidson [56], J.E. Davies [62], A. Davis [62], O. De Aguiar Francisco [62], C. De Angelis [31,l], F. De Benedetti [48], J. de Boer [37], K. De Bruyn [77], S. De Capua [62], M. De Cian [21,48], U. De Freitas Carneiro Da Graca [2,b], E. De Lucia [27], J.M. De Miranda [2], L. De Paula [3], M. De Serio [23,i], P. De Simone [27], F. De Vellis [19], J.A. de Vries [78], F. Debernardis [23], D. Decamp [10], V. Dedu [13], S. Dekkers [1], L. Del Buono [16], B. Delaney [64], H.-P. Dembinski [19], J. Deng [8], V. Denysenko [50], O. Deschamps [11], F. Dettori [31,l], B. Dey [76], P. Di Nezza [27], I. Diachkov [43], S. Didenko [43], S. Ding [68], L. Dittmann [21], V. Dobishuk [52], A. D. Docheva [59], C. Dong [4,c], A.M. Donohoe [22], F. Dordei [31], A.C. dos Reis [2], A. D. Dowling [68], W. Duan [71], P. Duda [79], M.W. Dudek [40], L. Dufour [48], V. Duk [33], P. Durante [48], M. M. Duras [79], J.M. Durham [67], O. D. Durmus [76], A. Dziurda [40], A. Dzyuba [43], S. Easo [57], E. Eckstein [18], U. Egede [1], A. Egorychev [43], V. Egorychev [43], S. Eisenhardt [58], E. Ejopu [62], L. Eklund [81], M. Elashri [65], J. Ellbracht [19], S. Ely [61], A. Ene [42], E. Epple [65], J. Eschle [68], S. Esen [21], T. Evans [62], F. Fabiano [31,l], L.N. Falcao [2], Y. Fan [7], B. Fang [73], L. Fantini [33,r,48], M. Faria [49], K. Farmer [58], D. Fazzini [30,p], L. Felkowski [79], M. Feng [5,7], M. Feo [19,48], A. Fernandez Casani [47], M. Fernandez Gomez [46], A.D. Fernez [66], F. Ferrari [24], F. Ferreira Rodrigues [3], M. Ferrillo [50], M. Ferro-Luzzi [48], S. Filippov [43], R.A. Fini [23], M. Fiorini [25,m], M. Firlej [39], K.L. Fischer [63], D.S. Fitzgerald [82], C. Fitzpatrick [62], T. Fiutowski [39], F. Fleuret [15], M. Fontana [24], L. F. Foreman [62], R. Forty [48], D. Foulds-Holt [55], V. Franco Lima [3], M. Franco Sevilla [66], M. Frank [48], E. Franzoso [25,m], G. Frau [62], C. Frei [48], D.A. Friday [62], J. Fu [7], Q. Führing [19,g,55], Y. Fujii [1], T. Fulghesu [16], E. Gabriel [37], G. Galati [23], M.D. Galati [37], A. Gallas Torreira [46], D. Galli [24,k], S. Gambetta [58], M. Gandelman [3], P. Gandini [29], B. Ganie [62], H. Gao [7], R. Gao [63], T.Q. Gao [55], Y. Gao [8], Y. Gao [6], Y. Gao[8], M. Garau [31,l], L.M. Garcia Martin [49], P. Garcia Moreno [45], J. García Pardiñas [48], K. G. Garg [8], L. Garrido [45], C. Gaspar [48], R.E. Geertsema [37], L.L. Gerken [19], E. Gersabeck [62], M. Gersabeck [62], T. Gershon [56], S. Ghizzo [28,n], Z. Ghorbanimoghaddam[54], L. Giambastiani [32,q], F. I. Giasemis [16,f], V. Gibson [55], H.K. Giemza [41], A.L. Gilman [63], M. Giovannetti [27], A. Gioventù [45], L. Girardey [62], P. Gironella Gironell [45], C. Giugliano [25,m], M.A. Giza [40], E.L. Gkougkousis [61], F.C. Glaser [14,21], V.V. Gligorov [16,48], C. Göbel [69], E. Golobardes [44], D. Golubkov [43], A. Golutvin [61,43,48], A. Gomes [2,a,†], S. Gomez Fernandez [45], F. Goncalves Abrantes [63], M. Goncerz [40], G. Gong [4,c], J. A. Gooding [19], I.V. Gorelov [43], C. Gotti [30], J.P. Grabowski [18], L.A. Granado Cardoso [48], E. Graugés [45], E. Graverini [49,t], L. Grazette [56], G. Graziani [], A. T. Grecu [42], L.M. Greeven [37], N.A. Grieser [65], L. Grillo [59], S. Gromov [43], C. Gu [15], M. Guarise [25], L. Guerry [11], M. Guittiere [14], V. Guliaeva [43], P. A. Günther [21], A.-K. Guseinov [49], E. Gushchin [43], Y. Guz [6,43,48], T. Gys [48], K. Habermann [18], T. Hadavizadeh [1], C. Hadjivasiliou [66], G. Haefeli [49], C. Haen [48], J. Haimberger [48], M. Hajheidari[48], G. Hallett [56], M.M. Halvorsen [48], P.M. Hamilton [66], J. Hammerich [60], Q. Han [8], X. Han [21], S. Hansmann-Menzemer [21], L. Hao [7], N. Harnew [63], M. Hartmann [14], S. Hashmi [39], J. He [7,d], F. Hemmer [48], C. Henderson [65], R.D.L. Henderson [1,56], A.M. Hennequin [48], K. Hennessy [60], L. Henry [49], J. Herd [61], P. Herrero Gascon [21], J. Heuel [17], A. Hicheur [3], G. Hijano Mendizabal[50], D. Hill [49], S.E. Hollitt [19], J. Horswill [62], R. Hou [8], Y. Hou [11], N. Howarth[60], J. Hu[21], J. Hu [71], W. Hu [6], X. Hu [4,c], W. Huang [7],

W. Hulsbergen [37], R.J. Hunter [56], M. Hushchyn [43], D. Hutchcroft [60], M. Idzik [39], D. Ilin [43], P. Ilten [65], A. Inglessi [43], A. Iniukhin [43], A. Ishteev [43], K. Ivshin [43], R. Jacobsson [48], H. Jage [17], S.J. Jaimes Elles [47,74], S. Jakobsen [48], E. Jans [37], B.K. Jashal [47], A. Jawahery [66,48], V. Jevtic [19], E. Jiang [66], X. Jiang [5,7], Y. Jiang [7], Y. J. Jiang [6], M. John [63], A. John Rubesh Rajan [22], D. Johnson [53], C.R. Jones [55], T.P. Jones [56], S. Joshi [41], B. Jost [48], J. Juan Castella [55], N. Jurik [48], I. Juszczak [40], D. Kaminaris [49], S. Kandybei [51], M. Kane [58], Y. Kang [4,c], C. Kar [11], M. Karacson [48], D. Karpenkov [43], A. Kauniskangas [49], J.W. Kautz [65], M.K. Kazanecki [40], F. Keizer [48], M. Kenzie [55], T. Ketel [37], B. Khanji [68], A. Kharisova [43], S. Kholodenko [34,48], G. Khreich [14], T. Kirn [17], V.S. Kirsebom [30,p], O. Kitouni [64], S. Klaver [38], N. Kleijne [34,s], K. Klimaszewski [41], M.R. Kmiec [41], S. Koliiev [52], L. Kolk [19], A. Konoplyannikov [43], P. Kopciewicz [39,48], P. Koppenburg [37], M. Korolev [43], I. Kostiuk [37], O. Kot [52], S. Kotriakhova [], A. Kozachuk [43], P. Kravchenko [43], L. Kravchuk [43], M. Kreps [56], P. Krokovny [43], W. Krupa [68], W. Krzemien [41], O. Kshyvanskyi [52], S. Kubis [79], M. Kucharczyk [40], V. Kudryavtsev [43], E. Kulikova [43], A. Kupsc [81], B. K. Kutsenko [13], D. Lacarrere [48], P. Laguarta Gonzalez [45], A. Lai [31], A. Lampis [31], D. Lancierini [55], C. Landesa Gomez [46], J.J. Lane [1], R. Lane [54], G. Lanfranchi [27], C. Langenbruch [21], J. Langer [19], O. Lantwin [43], T. Latham [56], F. Lazzari [34,t], C. Lazzeroni [53], R. Le Gac [13], H. Lee [60], R. Lefèvre [11], A. Leflat [43], S. Legotin [43], M. Lehuraux [56], E. Lemos Cid [48], O. Leroy [13], T. Lesiak [40], E. D. Lesser [48], B. Leverington [21], A. Li [4,c], C. Li [13], H. Li [71], K. Li [8], L. Li [62], M. Li [8], P. Li [7], P.-R. Li [72], Q. Li [5,7], S. Li [8], T. Li [5,e], T. Li [71], Y. Li [8], Y. Li [5], Z. Lian [4,c], X. Liang [68], S. Libralon [47], C. Lin [7], T. Lin [57], R. Lindner [48], V. Lisovskyi [49], R. Litvinov [31,48], F. L. Liu [1], G. Liu [71], K. Liu [72], S. Liu [5,7], W. Liu [8], Y. Liu [58], Y. Liu [72], Y. L. Liu [61], A. Lobo Salvia [45], A. Loi [31], J. Lomba Castro [46], T. Long [55], J.H. Lopes [3], A. Lopez Huertas [45], S. López Soliño [46], Q. Lu [15], C. Lucarelli [26], D. Lucchesi [32,q], M. Lucio Martinez [78], V. Lukashenko [37,52], Y. Luo [6], A. Lupato [32,j], E. Luppi [25,m], K. Lynch [22], X.-R. Lyu [7], G. M. Ma [4,c], R. Ma [7], S. Maccolini [19], F. Machefert [14], F. Maciuc [42], B. Mack [68], I. Mackay [63], L. M. Mackey [68], L.R. Madhan Mohan [55], M. J. Madurai [53], A. Maevskiy [43], D. Magdalinski [37], D. Maisuzenko [43], M.W. Majewski [39], J.J. Malczewski [40], S. Malde [63], L. Malentacca [48], A. Malinin [43], T. Maltsev [43], G. Manca [31,l], G. Mancinelli [13], C. Mancuso [29,14,o], R. Manera Escalero [45], D. Manuzzi [24], D. Marangotto [29,o], J.F. Marchand [10], R. Marchevski [49], U. Marconi [24], E. Mariani [16], S. Mariani [48], C. Marin Benito [45], J. Marks [21], A.M. Marshall [54], L. Martel [63], G. Martelli [33,r], G. Martellotti [35], L. Martinazzoli [48], M. Martinelli [30,p], D. Martinez Santos [46], F. Martinez Vidal [47], A. Massafferri [2], R. Matev [48], A. Mathad [48], V. Matiunin [43], C. Matteuzzi [68], K.R. Mattioli [15], A. Mauri [61], E. Maurice [15], J. Mauricio [45], P. Mayencourt [49], J. Mazorra de Cos [47], M. Mazurek [41], M. McCann [61], L. Mcconnell [22], T.H. McGrath [62], N.T. McHugh [59], A. McNab [62], R. McNulty [22], B. Meadows [65], G. Meier [19], D. Melnychuk [41], F. M. Meng [4,c], M. Merk [37,78], A. Merli [49], L. Meyer Garcia [66], D. Miao [5,7], H. Miao [7], M. Mikhasenko [75], D.A. Milanes [74], A. Minotti [30,p], E. Minucci [68], T. Miralles [11], B. Mitreska [19], D.S. Mitzel [19], A. Modak [57], R.A. Mohammed [63], R.D. Moise [17], S. Mokhnenko [43], E. F. Molina Cardenas [82], T. Mombächer [48], M. Monk [56,1], S. Monteil [11], A. Morcillo Gomez [46], G. Morello [27],

M.J. Morello [34,s], M.P. Morgenthaler [21], J. Moron [39], A.B. Morris [48], A.G. Morris [13],
R. Mountain [68], H. Mu [4,c], Z. M. Mu [6], E. Muhammad [56], F. Muheim [58], M. Mulder [77],
K. Müller [50], F. Muñoz-Rojas [9], R. Murta [61], P. Naik [60], T. Nakada [49], R. Nandakumar [57],
T. Nanut [48], I. Nasteva [3], M. Needham [58], N. Neri [29,o], S. Neubert [18], N. Neufeld [48],
P. Neustroev [43], J. Nicolini [19,14], D. Nicotra [78], E.M. Niel [49], N. Nikitin [43], P. Nogarolli [3],
P. Nogga [18], C. Normand [54], J. Novoa Fernandez [46], G. Nowak [65], C. Nunez [82], H. N.
Nur [59], A. Oblakowska-Mucha [39], V. Obraztsov [43], T. Oeser [17], S. Okamura [25,m],
A. Okhotnikov [43], O. Okhrimenko [52], R. Oldeman [31,l], F. Oliva [58], M. Olocco [19],
C.J.G. Onderwater [78], R.H. O'Neil [58], D. Osthues [19], J.M. Otalora Goicochea [3], P. Owen [50],
A. Oyanguren [47], O. Ozcelik [58], F. Paciolla [34,w], A. Padee [41], K.O. Padeken [18],
B. Pagare [56], P.R. Pais [21], T. Pajero [48], A. Palano [23], M. Palutan [27], G. Panshin [43],
L. Paolucci [56], A. Papanestis [57,48], M. Pappagallo [23,i], L.L. Pappalardo [25,m],
C. Pappenheimer [65], C. Parkes [62], B. Passalacqua [25], G. Passaleva [26], D. Passaro [34,s],
A. Pastore [23], M. Patel [61], J. Patoc [63], C. Patrignani [24,k], A. Paul [68], C.J. Pawley [78],
A. Pellegrino [37], J. Peng [5,7], M. Pepe Altarelli [27], S. Perazzini [24], D. Pereima [43], H.
Pereira Da Costa [67], A. Pereiro Castro [46], P. Perret [11], A. Perro [48], K. Petridis [54],
A. Petrolini [28,n], J. P. Pfaller [65], H. Pham [68], L. Pica [34,s], M. Piccini [33], L. Piccolo [31],
B. Pietrzyk [10], G. Pietrzyk [14], D. Pinci [35], F. Pisani [48], M. Pizzichemi [30,p,48], V. Placinta [42],
M. Plo Casasus [46], T. Poeschl [48], F. Polci [16,48], M. Poli Lener [27], A. Poluektov [13],
N. Polukhina [43], I. Polyakov [43], E. Polycarpo [3], S. Ponce [48], D. Popov [7], S. Poslavskii [43],
K. Prasanth [58], C. Prouve [46], D. Provenzano [31,l], V. Pugatch [52], G. Punzi [34,t], S. Qasim [50],
Q. Q. Qian [6], W. Qian [7], N. Qin [4,c], S. Qu [4,c], R. Quagliani [48], R.I. Rabadan Trejo [56],
J.H. Rademacker [54], M. Rama [34], M. Ramírez García [82], V. Ramos De Oliveira [69],
M. Ramos Pernas [56], M.S. Rangel [3], F. Ratnikov [43], G. Raven [38], M. Rebollo De Miguel [47],
F. Redi [29,j], J. Reich [54], F. Reiss [62], Z. Ren [7], P.K. Resmi [63], R. Ribatti [49], G. R.
Ricart [15,12], D. Riccardi [34,s], S. Ricciardi [57], K. Richardson [64], M. Richardson-Slipper [58],
K. Rinnert [60], P. Robbe [14], G. Robertson [59], E. Rodrigues [60], E. Rodriguez Fernandez [46],
J.A. Rodriguez Lopez [74], E. Rodriguez Rodriguez [46], J. Roensch [19], A. Rogachev [43],
A. Rogovskiy [57], D.L. Rolf [48], P. Roloff [48], V. Romanovskiy [65], M. Romero Lamas [46],
A. Romero Vidal [46], G. Romolini [25], F. Ronchetti [49], T. Rong [6], M. Rotondo [27], S. R.
Roy [21], M.S. Rudolph [68], M. Ruiz Diaz [21], R.A. Ruiz Fernandez [46], J. Ruiz Vidal [81,aa],
A. Ryzhikov [43], J. Ryzka [39], J. J. Saavedra-Arias [9], J.J. Saborido Silva [46], R. Sadek [15],
N. Sagidova [43], D. Sahoo [76], N. Sahoo [53], B. Saitta [31,l], M. Salomoni [30,48,p],
I. Sanderswood [47], R. Santacesaria [35], C. Santamarina Rios [46], M. Santimaria [27,48],
L. Santoro [2], E. Santovetti [36], A. Saputi [25,48], D. Saranin [43], A. Sarnatskiy [77], G. Sarpis [58],
M. Sarpis [62], C. Satriano [35,u], A. Satta [36], M. Saur [6], D. Savrina [43], H. Sazak [17],
F. Sborzacchi [48,27], L.G. Scantlebury Smead [63], A. Scarabotto [19], S. Schael [17], S. Scherl [60],
M. Schiller [59], H. Schindler [48], M. Schmelling [20], B. Schmidt [48], S. Schmitt [17], H. Schmitz [18],
O. Schneider [49], A. Schopper [48], N. Schulte [19], S. Schulte [49], M.H. Schune [14],
R. Schwemmer [48], G. Schwering [17], B. Sciascia [27], A. Sciuccati [48], S. Sellam [46],
A. Semennikov [43], T. Senger [50], M. Senghi Soares [38], A. Sergi [28,n,48], N. Serra [50],
L. Sestini [32], A. Seuthe [19], Y. Shang [6], D.M. Shangase [82], M. Shapkin [43], R. S. Sharma [68],
I. Shchemerov [43], L. Shchutska [49], T. Shears [60], L. Shekhtman [43], Z. Shen [6], S. Sheng [5,7],

V. Shevchenko [43], B. Shi [7], Q. Shi [7], Y. Shimizu [14], E. Shmanin [24], R. Shorkin [43], J.D. Shupperd [68], R. Silva Coutinho [68], G. Simi [32,q], S. Simone [23,i], N. Skidmore [56], T. Skwarnicki [68], M.W. Slater [53], J.C. Smallwood [63], E. Smith [64], K. Smith [67], M. Smith [61], A. Snoch [37], L. Soares Lavra [58], M.D. Sokoloff [65], F.J.P. Soler [59], A. Solomin [43,54], A. Solovev [43], I. Solovyev [43], R. Song [1], Y. Song [49], Y. Song [4,c], Y. S. Song [6], F.L. Souza De Almeida [68], B. Souza De Paula [3], E. Spadaro Norella [28,n], E. Spedicato [24], J.G. Speer [19], E. Spiridenkov [43], P. Spradlin [59], V. Sriskaran [48], F. Stagni [48], M. Stahl [48], S. Stahl [48], S. Stanislaus [63], E.N. Stein [48], O. Steinkamp [50], O. Stenyakin [43], H. Stevens [19], D. Strekalina [43], Y. Su [7], F. Suljik [63], J. Sun [31], L. Sun [73], Y. Sun [66], D. Sundfeld [2], W. Sutcliffe [50], P.N. Swallow [53], K. Swientek [39], F. Swystun [55], A. Szabelski [41], T. Szumlak [39], Y. Tan [4,c], M.D. Tat [63], A. Terentev [43], F. Terzuoli [34,w,48], F. Teubert [48], E. Thomas [48], D.J.D. Thompson [53], H. Tilquin [61], V. Tisserand [11], S. T'Jampens [10], M. Tobin [5,48], L. Tomassetti [25,m], G. Tonani [29,o,48], X. Tong [6], D. Torres Machado [2], L. Toscano [19], D.Y. Tou [4,c], C. Trippl [44], G. Tuci [21], N. Tuning [37], L.H. Uecker [21], A. Ukleja [39], D.J. Unverzagt [21], E. Ursov [43], A. Usachov [38], A. Ustyuzhanin [43], U. Uwer [21], V. Vagnoni [24], V. Valcarce Cadenas [46], G. Valenti [24], N. Valls Canudas [48], H. Van Hecke [67], E. van Herwijnen [61], C.B. Van Hulse [46,y], R. Van Laak [49], M. van Veghel [37], G. Vasquez [50], R. Vazquez Gomez [45], P. Vazquez Regueiro [46], C. Vázquez Sierra [46], S. Vecchi [25], J.J. Velthuis [54], M. Veltri [26,x], A. Venkateswaran [49], M. Verdoglia [31], M. Vesterinen [56], D. Vico Benet [63], P. Vidrier Villalba [45], M. Vieites Diaz [48], X. Vilasis-Cardona [44], E. Vilella Figueras [60], A. Villa [24], P. Vincent [16], F.C. Volle [53], D. vom Bruch [13], N. Voropaev [43], K. Vos [78], G. Vouters [10], C. Vrahas [58], J. Wagner [19], J. Walsh [34], E.J. Walton [1,56], G. Wan [6], C. Wang [21], G. Wang [8], J. Wang [6], J. Wang [5], J. Wang [4,c], J. Wang [73], M. Wang [29], N. W. Wang [7], R. Wang [54], X. Wang [8], X. Wang [71], X. W. Wang [61], Y. Wang [6], Z. Wang [14], Z. Wang [4,c], Z. Wang [29], J.A. Ward [56,1], M. Waterlaat [48], N.K. Watson [53], D. Websdale [61], Y. Wei [6], J. Wendel [80], B.D.C. Westhenry [54], C. White [55], M. Whitehead [59], E. Whiter [53], A.R. Wiederhold [62], D. Wiedner [19], G. Wilkinson [63], M.K. Wilkinson [65], M. Williams [64], M.R.J. Williams [58], R. Williams [55], Z. Williams [54], F.F. Wilson [57], W. Wislicki [41], M. Witek [40], L. Witola [21], G. Wormser [14], S.A. Wotton [55], H. Wu [68], J. Wu [8], Y. Wu [6], Z. Wu [7], K. Wyllie [48], S. Xian [71], Z. Xiang [5], Y. Xie [8], A. Xu [34], J. Xu [7], L. Xu [4,c], L. Xu [4,c], M. Xu [56], Z. Xu [48], Z. Xu [7], Z. Xu [5], D. Yang [4], K. Yang [61], S. Yang [7], X. Yang [6], Y. Yang [28,n], Z. Yang [6], Z. Yang [66], V. Yeroshenko [14], H. Yeung [62], H. Yin [8], X. Yin [7], C. Y. Yu [6], J. Yu [70], X. Yuan [5], Y Yuan [5,7], E. Zaffaroni [49], M. Zavertyaev [20], M. Zdybal [40], F. Zenesini [24,k], C. Zeng [5,7], M. Zeng [4,c], C. Zhang [6], D. Zhang [8], J. Zhang [7], L. Zhang [4,c], S. Zhang [70], S. Zhang [63], Y. Zhang [6], Y. Z. Zhang [4,c], Y. Zhao [21], A. Zharkova [43], A. Zhelezov [21], S. Z. Zheng [6], X. Z. Zheng [4,c], Y. Zheng [7], T. Zhou [6], X. Zhou [8], Y. Zhou [7], V. Zhovkovska [56], L. Z. Zhu [7], X. Zhu [4,c], X. Zhu [8], V. Zhukov [17], J. Zhuo [47], Q. Zou [5,7], D. Zuliani [32,q], G. Zunica [49]

[1] School of Physics and Astronomy, Monash University, Melbourne, Australia

[2] Centro Brasileiro de Pesquisas Físicas (CBPF), Rio de Janeiro, Brazil

[3] Universidade Federal do Rio de Janeiro (UFRJ), Rio de Janeiro, Brazil

[4] Department of Engineering Physics, Tsinghua University, Beijing, China

[5] Institute Of High Energy Physics (IHEP), Beijing, China

[6] School of Physics State Key Laboratory of Nuclear Physics and Technology, Peking University, Beijing, China

[7] *University of Chinese Academy of Sciences, Beijing, China*

[8] *Institute of Particle Physics, Central China Normal University, Wuhan, Hubei, China*

[9] *Consejo Nacional de Rectores (CONARE), San Jose, Costa Rica*

[10] *Université Savoie Mont Blanc, CNRS, IN2P3-LAPP, Annecy, France*

[11] *Université Clermont Auvergne, CNRS/IN2P3, LPC, Clermont-Ferrand, France*

[12] *Université Paris-Saclay, Centre d'Etudes de Saclay (CEA), IRFU, Saclay, France, Gif-Sur-Yvette, France*

[13] *Aix Marseille Univ, CNRS/IN2P3, CPPM, Marseille, France*

[14] *Université Paris-Saclay, CNRS/IN2P3, IJCLab, Orsay, France*

[15] *Laboratoire Leprince-Ringuet, CNRS/IN2P3, Ecole Polytechnique, Institut Polytechnique de Paris, Palaiseau, France*

[16] *LPNHE, Sorbonne Université, Paris Diderot Sorbonne Paris Cité, CNRS/IN2P3, Paris, France*

[17] *I. Physikalisches Institut, RWTH Aachen University, Aachen, Germany*

[18] *Universität Bonn - Helmholtz-Institut für Strahlen und Kernphysik, Bonn, Germany*

[19] *Fakultät Physik, Technische Universität Dortmund, Dortmund, Germany*

[20] *Max-Planck-Institut für Kernphysik (MPIK), Heidelberg, Germany*

[21] *Physikalisches Institut, Ruprecht-Karls-Universität Heidelberg, Heidelberg, Germany*

[22] *School of Physics, University College Dublin, Dublin, Ireland*

[23] *INFN Sezione di Bari, Bari, Italy*

[24] *INFN Sezione di Bologna, Bologna, Italy*

[25] *INFN Sezione di Ferrara, Ferrara, Italy*

[26] *INFN Sezione di Firenze, Firenze, Italy*

[27] *INFN Laboratori Nazionali di Frascati, Frascati, Italy*

[28] *INFN Sezione di Genova, Genova, Italy*

[29] *INFN Sezione di Milano, Milano, Italy*

[30] *INFN Sezione di Milano-Bicocca, Milano, Italy*

[31] *INFN Sezione di Cagliari, Monserrato, Italy*

[32] *INFN Sezione di Padova, Padova, Italy*

[33] *INFN Sezione di Perugia, Perugia, Italy*

[34] *INFN Sezione di Pisa, Pisa, Italy*

[35] *INFN Sezione di Roma La Sapienza, Roma, Italy*

[36] *INFN Sezione di Roma Tor Vergata, Roma, Italy*

[37] *Nikhef National Institute for Subatomic Physics, Amsterdam, Netherlands*

[38] *Nikhef National Institute for Subatomic Physics and VU University Amsterdam, Amsterdam, Netherlands*

[39] *AGH - University of Krakow, Faculty of Physics and Applied Computer Science, Kraków, Poland*

[40] *Henryk Niewodniczanski Institute of Nuclear Physics Polish Academy of Sciences, Kraków, Poland*

[41] *National Center for Nuclear Research (NCBJ), Warsaw, Poland*

[42] *Horia Hulubei National Institute of Physics and Nuclear Engineering, Bucharest-Magurele, Romania*

[43] *Affiliated with an institute covered by a cooperation agreement with CERN*

[44] *DS4DS, La Salle, Universitat Ramon Llull, Barcelona, Spain*

[45] *ICCUB, Universitat de Barcelona, Barcelona, Spain*

[46] *Instituto Galego de Física de Altas Enerxías (IGFAE), Universidade de Santiago de Compostela, Santiago de Compostela, Spain*

[47] *Instituto de Fisica Corpuscular, Centro Mixto Universidad de Valencia - CSIC, Valencia, Spain*

[48] *European Organization for Nuclear Research (CERN), Geneva, Switzerland*

[49] *Institute of Physics, Ecole Polytechnique Fédérale de Lausanne (EPFL), Lausanne, Switzerland*

[50] *Physik-Institut, Universität Zürich, Zürich, Switzerland*

[51] *NSC Kharkiv Institute of Physics and Technology (NSC KIPT), Kharkiv, Ukraine*

[52] *Institute for Nuclear Research of the National Academy of Sciences (KINR), Kyiv, Ukraine*

[53] *School of Physics and Astronomy, University of Birmingham, Birmingham, United Kingdom*

[54] *H.H. Wills Physics Laboratory, University of Bristol, Bristol, United Kingdom*

[55] *Cavendish Laboratory, University of Cambridge, Cambridge, United Kingdom*

[56] *Department of Physics, University of Warwick, Coventry, United Kingdom*

[57] *STFC Rutherford Appleton Laboratory, Didcot, United Kingdom*

[58] *School of Physics and Astronomy, University of Edinburgh, Edinburgh, United Kingdom*

[59] *School of Physics and Astronomy, University of Glasgow, Glasgow, United Kingdom*

[60] *Oliver Lodge Laboratory, University of Liverpool, Liverpool, United Kingdom*

[61] *Imperial College London, London, United Kingdom*

[62] *Department of Physics and Astronomy, University of Manchester, Manchester, United Kingdom*

[63] *Department of Physics, University of Oxford, Oxford, United Kingdom*

[64] *Massachusetts Institute of Technology, Cambridge, MA, United States*

[65] *University of Cincinnati, Cincinnati, OH, United States*

[66] *University of Maryland, College Park, MD, United States*

[67] *Los Alamos National Laboratory (LANL), Los Alamos, NM, United States*

[68] *Syracuse University, Syracuse, NY, United States*

[69] *Pontifícia Universidade Católica do Rio de Janeiro (PUC-Rio), Rio de Janeiro, Brazil, associated to [3]*

[70] *School of Physics and Electronics, Hunan University, Changsha City, China, associated to [8]*

[71] *Guangdong Provincial Key Laboratory of Nuclear Science, Guangdong-Hong Kong Joint Laboratory of Quantum Matter, Institute of Quantum Matter, South China Normal University, Guangzhou, China, associated to [4]*

[72] *Lanzhou University, Lanzhou, China, associated to [5]*

[73] *School of Physics and Technology, Wuhan University, Wuhan, China, associated to [4]*

[74] *Departamento de Fisica , Universidad Nacional de Colombia, Bogota, Colombia, associated to [16]*

[75] *Ruhr Universitaet Bochum, Fakultaet f. Physik und Astronomie, Bochum, Germany, associated to [19]*

[76] *Eotvos Lorand University, Budapest, Hungary, associated to [48]*

[77] *Van Swinderen Institute, University of Groningen, Groningen, Netherlands, associated to [37]*

[78] *Universiteit Maastricht, Maastricht, Netherlands, associated to [37]*

[79] *Tadeusz Kosciuszko Cracow University of Technology, Cracow, Poland, associated to [40]*

[80] *Universidade da Coruña, A Coruña, Spain, associated to [44]*

[81] *Department of Physics and Astronomy, Uppsala University, Uppsala, Sweden, associated to [59]*

[82] *University of Michigan, Ann Arbor, MI, United States, associated to [68]*

[a] *Universidade de Brasília, Brasília, Brazil*

[b] *Centro Federal de Educacão Tecnológica Celso Suckow da Fonseca, Rio De Janeiro, Brazil*

[c] *Center for High Energy Physics, Tsinghua University, Beijing, China*

[d] *Hangzhou Institute for Advanced Study, UCAS, Hangzhou, China*

[e] *School of Physics and Electronics, Henan University , Kaifeng, China*

[f] *LIP6, Sorbonne Université, Paris, France*

[g] *Lamarr Institute for Machine Learning and Artificial Intelligence, Dortmund, Germany*

[h] *Universidad Nacional Autónoma de Honduras, Tegucigalpa, Honduras*

[i] *Università di Bari, Bari, Italy*

[j] *Università di Bergamo, Bergamo, Italy*

[k] *Università di Bologna, Bologna, Italy*

[l] *Università di Cagliari, Cagliari, Italy*

[m] *Università di Ferrara, Ferrara, Italy*

[n] *Università di Genova, Genova, Italy*

[o] *Università degli Studi di Milano, Milano, Italy*

[p] *Università degli Studi di Milano-Bicocca, Milano, Italy*

[q] *Università di Padova, Padova, Italy*

[r] *Università di Perugia, Perugia, Italy*

[s] *Scuola Normale Superiore, Pisa, Italy*

[t] *Università di Pisa, Pisa, Italy*

[u] *Università della Basilicata, Potenza, Italy*

[v] *Università di Roma Tor Vergata, Roma, Italy*

[w] *Università di Siena, Siena, Italy*

[x] *Università di Urbino, Urbino, Italy*

[y] *Universidad de Alcalá, Alcalá de Henares , Spain*

[z] *Facultad de Ciencias Fisicas, Madrid, Spain*

[aa] *Department of Physics/Division of Particle Physics, Lund, Sweden*

[†] *Deceased*